Silesian University of Technology
Faculty of Mechanical Engineering
Institute of Engineering Processes Automation
and Integrated Manufacturing Systems

SELECTED ENGINEERING PROBLEMS

NUMBER 7

Gliwice 2016

Articles published on the basis of materials supplied by the authors.

ISSN 2299-954X

CONTENTS

SELECTED ENGINEERING PROBLEMS
NUMBER 7
INSTITUTE OF ENGINEERING PROCESSES AUTOMATION
AND INTEGRATED MANUFACTURING SYSTEMS

Andrzej BAIER, Julia NOJEK*

Institute of Engineering Processes Automation and Integrated Manufacturing Systems, Faculty of Mechanical Engineering, Silesian University of Technology, Gliwice, Poland
* julia.nojek@gmail.com

POSSIBLE APPLICATION OF ARTIFICIAL SHARK SKIN AS SURFACE REDUCTING AERODYNAMIC DRAG

Abstract: In this paper the possibility of using artificial shark skin in order to improve aerodynamics of Silesian Greenpower race car is considered. Strong evidences, that this synthetic product should be applied on the surface of the Greenpowers car sheathing are presented.

1. Introduction

Aerodynamics of vehicles is one of the most important areas in their design - appropriate selection of parameters allows to reduce air resistance and thus significantly increase the speed and economics of travel. This area is part of the fluid mechanic, which also includes hydrodynamics. These two issues, aerodynamics and hydrodynamics vary from each other with environment where the research is carried. Air has lower viscosity in comparison to liquid and it is about 64 times less viscous than water, but aqueous media are not as compressible as air [1].
Despite occurring differences aerodynamic drag can be described by the following equation:

$$R = \frac{1}{2}\rho C A v^2, \tag{1}$$

where: R – aerodynamic drag, ρ - density of the medium, C – coefficient depending on the shape of the object, A – sectional area of the body, v - speed of the body relative to the medium.

Based on the equation (1) which can be used either in aerodynamics and in hydrodynamics it was decided to show common parts of this two areas and their application [1,2].

The signs of this law can be seen in animal kingdom, especially in water environment. A lot of animals possess features allowing them to swim faster. And it is not only the streamline shape of their bodies, but also scales or denticles, which are characteristic for sharks.

Shark skin is not smooth like for example dolphins' one but covered with structures similar to small teeth placed all over them (Fig.1.). That structure of scales permit these animals to reduce the viscosity of water by breaking up water vortices that would otherwise create drag. This attribute of this predatory fish is used in different areas – Speedo Fastskin is

one of the best examples. It is product from Speedo, company manufacturing swim accessories, which takes advantages of shark skin and covers the surface of suit with small v-shaped channels being the projection of animal denticles. This shows the possibilities of recreating such structures – one can see difference between real and artificial shark skin in Fig.1. and Fig.2., respectively [5,6,7].

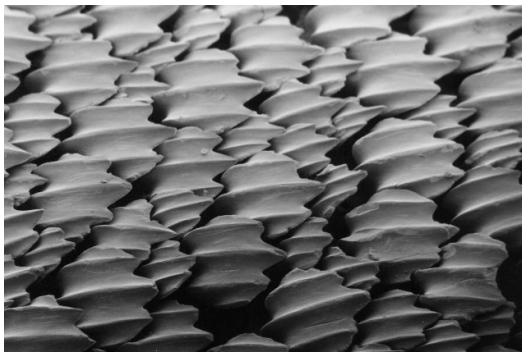

Fig.1. Magnified shark skin [3]

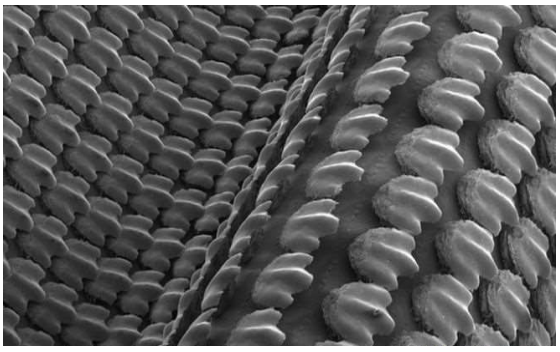

Fig.2. Close up of synthetic shark skin [4]

2. Results of simulations of synthetic shark skin and Greenpower race car

Synthetic shark skin (Fig.2.) manufactured with multimaterial 3D printing has been tested using different parameters.

In the following two tables are shown received results presenting the dependence of static drag force and drag reduction percentage on channel flow speed, Reynolds number and S+; also power consumption and costs of transport of synthetic shark skin and smooth membranes under various motion programs [4].

Tab. 1. Dependence of static drag force and drag reduction percentage on channel flow speed, Reynolds number and S+[4]

				Drag force		
Water tank flow speed ($m\,s^{-1}$)	Re_{ch} ($\times 10^3$)	Re_c ($\times 10^3$)	Turbulent $S+$	Synthetic shark skin (mN)	Smooth membrane (mN)	Drag reduction (%)
0.129	32.31	9.94	5.61	7.59±0.42	8.31±0.19	8.72
0.194	48.47	14.95	8.09	19.26±0.48	20.02±0.46	3.79
0.258	64.63	19.88	10.46	36.26±0.55	37.46±0.37	3.20
0.323	80.78	24.89	12.80	58.84±0.60	60.16±0.71	2.19
0.387	96.94	29.83	15.07	89.88±1.55	86.58±0.31	−3.81
0.452	113.09	34.83	17.33	129.72±1.40	119.93±0.37	−8.16
0.517	129.25	39.85	19.55	178.0±1.22	159.5±1.21	−11.60
0.581	145.41	44.77	21.72	241.58±2.86	209.90±0.59	−15.09

For definitions of channel Reynolds number (Re_{ch}), chord Reynolds number (Re_c) and turbulent $S+$, see Materials and methods.
Static drag force data consist of eight water tank flow speed points taken between 0.129 and 0.581 $m\,s^{-1}$ at increments of 0.065 $m\,s^{-1}$. Negative drag reduction values in the last column indicate that the shark skin membrane had enhanced drag relative to the smooth model. Drag force measurements are the means of N=5 replicate trials; error values are ±1 s.e.m.

Tables shown above prove that using shark skin denticles like structure coating can lead to reduction of the drag up to 15% and at the same time to reduction of the costs of transport. With such results it can be established that covering places on race car sheathing particularly vulnerable to aerodynamic drag could improve the reduction of drag force.

Taking findings below (Fig.3., Fig.4.) of the Silesian Greenpower race car ANSYS simulation it can be shown that there are areas placed on the car which generate higher aerodynamic drag.

Tab. 2. Power consumption and cost of transport of synthetic skin and smooth membranes under various motion programs[4]

	Total power (mW)		COT (J m^{-1} kg^{-1})			
Motion program	Shark skin	Smooth	Shark skin	Smooth	Power reduction (%)	COT reduction (%)
f=1 Hz, *h*=±1 cm	9.23±0.22	9.75±0.16	1.22±0.03	1.26±0.02	5.54	3.18
f=1 Hz, *h*=±2.5 cm	89.4±0.38	88.3±0.49	5.08±0.02	5.25±0.03	−1.24	3.26
f=1.5 Hz, *h*=±1 cm	39.3±0.27	39.15±0.36	2.64±0.02	2.81±0.03	−0.38	5.87
f=2.5 Hz, *h*=±1 cm	114.28±0.49	121.05±1.55	5.46±0.02	5.64±0.07	5.60	3.14
f=1 Hz, *h*=±1.5 cm, θ=10 deg	17.57±0.09	17.67±0.10	1.17±0.01	1.235±0.01	0.57	5.11
f=1 Hz, *h*=±1.5 cm, θ=30 deg	77.93±0.50	76.88±0.82	6.48±0.04	6.39±0.07	−1.37	−1.40

COT, cost of transport; *f*, frequency; *h*, heave; θ, pitch.
Total power (heave power + pitch power, per flapping cycle), and COT data are shown. All power and COT results are the mean of *N*=5 replicate trials for each measurement; error values are ±1 s.e.m.

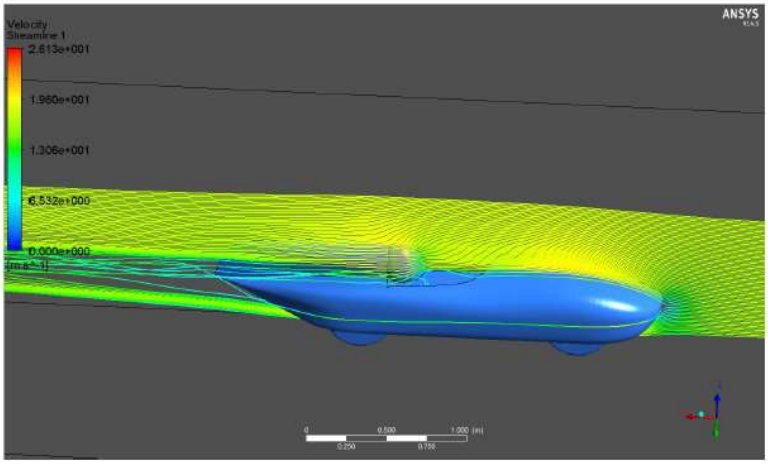

Fig.3. The course of streams of air around the race car SG2013[8]

In Fig.3. air streams around the rear of the vehicle and the rear fairing can be exactly seen.

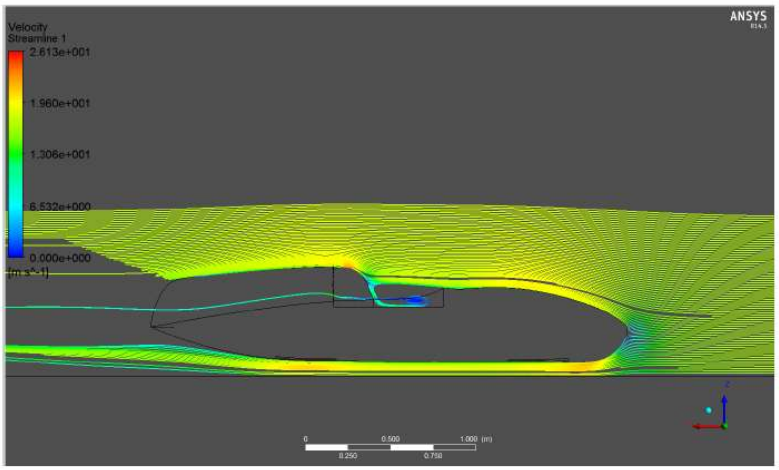

Fig. 4. The course of streams of air around the race car SG2013 [8]

Air circulation against the helmet is visible - the gas repeatedly rotates inside the driver's cab and then leaves it on the one side of driver's helmet. While leaving the cockpit it also interacts with air, at higher speed, and then moves directly from the front of the vehicle and cause turbulent behavior. Under this conditions it results in multiple air change of velocity of flow. Irregular and rough flow is unfavorable and leads to increasement of aerodynamic drag [8,9].

3. Conclusion

As a result of research conducted on the coating with shark skin denticles and smooth coating and comparing the results received from simulation environment with the same parametres for both, it was found that it is possible to reduce transport costs and energy consumption resulting from the reduction of aerodynamic drag forces.

Artificial shark skin inspired surface on the shell of the car would allow to: spread out air stream, reduce the viscosity of the air and transfer the positive effects of the applied coating in relation to the vehicle. The difference between the density and viscosity of the centers, which were conducted simulations require further testing issues, but because both are considered fluids, it can be a significant improvement in aerodynamics of the vehicle.

References

1. Piechna J.: The Basics of Vehicles Aerodynamics (in Polish), Wydawnictwo Komunikacji i Łączności, Warsaw, 2000.
2. Baier A., Baier M., Dusik D., Grabowski L., Miera A., Papaj P., Sobek M.: Computer aided process of designing the mechatronic Silesian Greenpower electric car, Selected Engineering Problems, 2013, pp. 13 – 18.
3. Wen L., Weaver J.C., Lauder G.V.: Biomimetic shark skin: design, fabrication and hydrodynamic function, „Journal of Experimental Biology" 2014, Vol.217 no.10, pp. 1656 – 1666. Access on 16.11.2016.
4. Harper J.W.: What are the Fastest Swimmers on Earth, USMS SWIMMER, September – October 2007, pp. 36 – 39, Access on 16.11.2016.
5. http://www.speedo.co.uk/technology/fastskin, Access on 16.11.2016.
6. http://www.explainthatstuff.com/biomimeticclothing.html, Access on 16.11.2016.
7. Grabowski L.: Application of CAD/CAE class systems to aerodynamic analysis of Greenpower race cars, Promotor Krzysztof Herbus , Working Diploma Thesis, Silesian University of Technology, 2014 (in Polish), pp. 55 – 62.
8. Grabowski L., Baier A., Buchacz A., Majzner M., Sobek M.: Application of CAD/CAE class systems to aerodynamic analysis of electric race cars, 2015, IOP Conf. Series: Materials Science and Engineering 95 012044.

SELECTED ENGINEERING PROBLEMS
NUMBER7
INSTITUTE OF ENGINEERING PROCESSES AUTOMATION
AND INTEGRATED MANUFACTURING SYSTEMS

Marek GODZWA[1]

[1] Faculty of Automatic Control, Electronics, and Computer Science,
Silesian University of Technology, Akademicka 16 Street, 44-100 Gliwice Poland.
*godzwa@pi.pl

ROBOT SX-300 EQUATION, WITH USING NEW GAUSS AND PARAMETRIC METHOD

Abstract: Process of calculation robot Adept SX-300 equation can start from calculation matrix T6 result. My new version of Gauss method take possibility calculate vector of corners, for less complicated equations. For very complicate T6 results, is need additional using parametric method, which can take control values, that are unchanged at the moment of calculation, such as parameters of solution, like constant values. Quality of this solution is very high, and error of calculation is smaller to diameter of electron in hydrogen atom.

1. Introduction

For take robot Adept SX-300 arm function, using T6 method, is need calculate result of translation. Generally, matrix of vectors, on right matrix column, define grapple location. Consist usually, in result, in first line, mostly cosine function, and in second line sine function.

Its correspond to projection on horizontal axis in first line, and vertical axis in second:

$$\begin{aligned} l1*\cos\theta_1 + l2*\cos\theta_2 + l3*\cos\theta_3 + ... = L \\ l1*\sin\theta_1 + l2*\sin\theta_2 + l3*\sin\theta_3 + ... = H \end{aligned} . \tag{1}$$

Create Gauss matrix:

$$\begin{bmatrix} l1*\cos\theta_1 & l2*\cos\theta_2 & l3*\cos\theta_3 & ....|L \\ l1*\sin\theta_1 & l2*\sin\theta_2 & l3*\sin\theta_3 & ....|H \end{bmatrix} . \tag{2}$$

After raise to the second power, both lines, and adding by sides, we obtain result:

$$\begin{aligned} &l1^2*(\cos^2\theta_1 + \sin^2\theta_1) + l2^2*(...) + l3^2*(...) + ... + 2*l1*l2*\cos\theta_1*\cos\theta_2 + ... \\ &+2*l1*l2*\sin\theta_1*\sin\theta_2 + ... = L^2 + H^2 \end{aligned} \tag{3}$$

After moving constant, on right side:

$$2*l1*l2*(\cos\theta_1*\cos\theta_2+\sin\theta_1*\sin\theta_2)+....=L^2+H^{'}-l1^2-l2^2-l3^2-... \quad (4)$$

After substitution formula: cos (α - β) = cosα*cosβ + sinα*sinβ, we obtain result:

$$2*l1*l2*\cos(\theta_1-\theta_2)+....=L^2+H^{'}-l1^2-l2^2-l3^2-... \quad (5)$$

For only two corners:

$$\cos(\theta_1-\theta_2)=\frac{L^2+H^2-l1^2-l2^2}{2*l1*l2}. \quad (6)$$

For sample, input matrix:

$$\left[\begin{array}{ccc|c} l1*\cos\theta_1 & l2*\cos\theta_2 & l3 & L \\ l1*\sin\theta_1 & l2*\sin\theta_2 & -l4 & H \end{array}\right]. \quad (7)$$

This formula will have form:

$$\cos(\theta_1-\theta_2)=\frac{(L-l3)^2+(H+l4)^2-l1^2-l2^2}{2*l1*l2}. \quad (8)$$

2. Introduction, and apply parametric method

For the same sample of equation, we move constants on right side:

$$\left[\begin{array}{ccc} l1*\cos\theta_1 & l2*\cos\theta_2 & L-l3 \\ l1*\sin\theta_1 & l2*\sin\theta_2 & H+l4 \end{array}\right]. \quad (9)$$

For right side we can make new value b1 and b2:

b1= L-l3,

b2= H+l4.

For this values result will equal:

$$\cos(\theta_1-\theta_2)=\frac{b1^2+b2^2-l1^2-l2^2}{2*l1*l2}. \quad (10)$$

End now to this values we can take all corners witch not change in time of calculation.
For more complicated matrix T6:

$$\begin{bmatrix} C1*C234 & -C1*S234*S5-S1*C5 & -C1*S234*C5+S1*S5 & \text{C1*(S234*C5*l4+C234*l3+C23*l2+C2*l1)-S1*S5*l4+C1*l0} \\ \text{S1*C234} & \text{-S1*S234*S5+C1*C5} & \text{-S1*S234*C5-C1*S5} & \text{S1*(S234*C5*l4+C234*l3+C23*l2+C2*l1)+C1*S5*l4+S1*l0} \\ S234 & C234*S5 & C234*C5 & \text{-C234*C5*l4+S234*l3+S23*l2+S2*l1+h0} \\ 0 & 0 & 0 & 1 \end{bmatrix}. \quad (11)$$

We can build Gauss Matrix:

$$\left[\begin{array}{cccccc|c} -S1*S6*l4 & C1*S234*C6*l4 & C1*C234*l3 & C1*C23*l2 & C1*C2*l1 & C1*l0 & L \\ C1*S6*l4 & S1*S234*C6*l4 & S1*C234*l3 & S1*C23*l2 & S1*C2*l1 & S1*l0 & Y \\ 0 & -C234*C6*l4 & S234*l3 & S23*l2 & S2*l1 & h0 & H \\ 0 & 0 & 0 & 0 & 0 & 1 & 1 \end{array}\right]. \quad (12)$$

We can divide first line by C1, and second by S1:

$$\left[\begin{array}{cccccc|c} -S1*S6*l4/C1 & S234*C6*l4 & C234*l3 & C23*l2 & C2*l1 & l0 & L/C1 \\ C1*S6*l4/S1 & S234*C6*l4 & C234*l3 & C23*l2 & C2*l1 & l0 & Y/S1 \\ 0 & -C234*C6*l4 & S234*l3 & S23*l2 & S2*l1 & h0 & H \\ 0 & 0 & 0 & 0 & 0 & 1 & 1 \end{array}\right]. \quad (13)$$

In next step we can move constants, and parameters on right side equation:

$$\left[\begin{array}{cc|c} C23*l2 & C2*l1 & L/\text{C1}+S1*S6*l4/C1-C234*13-l0 \\ C23*l2 & C2*l1 & Y/\text{S1}-C1*S6*l4/S1-C234*13-l0 \\ S23*l2 & S2*l1 & H-C234*C6*l4-S234*13-h0 \\ 0 & 1 & 1 \end{array}\right]. \quad (14)$$

We can take, like before, new values b1 and b2:

$$\text{b1= L/C1 + S1*S6*l4/C1 – C234*l3 – l0,} \quad (15)$$

$$\text{b2= H – C234*C6*l4 – S234*l3 – h0.}$$

We can use solution (10) from my version of Gauss method:

$$\cos(\theta_1-\theta_2)=\frac{b1^2+b2^2-l1^2-l2^2}{2*l1*l2}. \quad (16)$$

As solution we have:

$$\Theta\text{2-}\Theta\text{23} = \Theta\text{2} - \Theta\text{2} + \Theta\text{3} = \Theta\text{3}, \quad (17)$$

$$\theta_3 = a\cos\left(\frac{(L/C1+S1*S6*l4/C1-C234*l3-l0)^2+(H-C234*C6*l4-S234*l3-h0)^2-l1^2-l2^2}{2*l1*l2}\right).$$

Calculation Θ2.

The same we can make with equation (14), for calculation Θ2:

$$C2 = \frac{b1*a1 \; - \; b2*a2}{a1^2 + a2^2}. \tag{18}$$

For a1= l1+l2*C3 and a2=l2*S3:

$$C2 = \frac{b1*(l1 + l2*C3) \; - \; b2*S3*l2}{(l1 + l2*C3)^2 + (S3*l2)^2}. \tag{19}$$

When we using b1, and b2 full values: (20)

$$\Theta 2 = a\cos\left(\frac{(L/C1 + S1*S6*l4/S1 - C234*l3 - l0)*(l1 + l2*C3) - (H - C234*C6*l4 - S234*l3 - h0)*S3*l2}{(l1 + l2*C3)^2 + (S3*l2)^2}\right).$$

Calculation Θ1.

For calculation Θ1 we can return to first Gauss matrix (12),

$$\left[\begin{array}{cccccc|c} -S1*S6*l4 & C1*S234*C6*l4 & C1*C234*l3 & C1*C23*l2 & C1*C2*l1 & C1*l0 & L \\ C1*S6*l4 & S1*S234*C6*l4 & S1*C234*l3 & S1*C23*l2 & S1*C2*l1 & S1*l0 & Y \\ 0 & -C234*C6*l4 & S234*l3 & S23*l2 & S2*l1 & h0 & H \\ 0 & 0 & 0 & 0 & 0 & 1 & 1 \end{array}\right], \tag{21}$$

and to first two lines, we can take new value a3=S234*C6*l4+C234*l3+C23*l2+C2*l1+l0

$$\left[\begin{array}{cc|c} -S1*S6*l4 & C1*a3 & L \\ C1*S6*l4 & S1*a3 & Y \end{array}\right]. \tag{22}$$

After calculation by my version Gauss method:

$$S6^2*l4^2 + a3^2 - 2*S1*C1*S6*l4*a3 + 2*S1*C1*S6*l4*a3 = L^2 + Y^2,$$

$$a3 = \sqrt{L^2 + Y^2 - S6^2*l4^2}. \tag{23}$$

And after simply calculation S1 value from (22):

$$S1 = \frac{Y*a3 \; - \; L*S6*l4}{S6^2*l4^2 + \; a3^2}. \tag{24}$$

We can take a3 value to equation:

$$\Theta 1 = a\sin(\frac{Y*\sqrt{L^2+Y^2-S6^2*l4^2}-L*S6*l4}{L^2+Y^2}). \quad (25)$$

In result we have calculated corners Θ1, Θ2, Θ3.

Removing discontinuity.

For removing discontinuity, we can return to value b1 (15).

$$b1= L/C1 + S1*S6*l4/C1 – C234*l3 – l0.$$

Value b1, for corner Θ1= ±90° is going to infinity. For solve this problem, we can see on value a3 in first line of matrix, in calculation a3 (22):

$$-S1*S6*l4 + C1*a3 = L. \quad (26)$$

We can calculate a3:

$$a3 = L/C1 + S1*S6*l4/C1. \quad (27)$$

This two discontinuity elements, are equal to a3, and on his place we can take a3 value. In result b1 will change to:

$$b1 = \sqrt{L^2+Y^2-S6^2*l4^2} - C234*l3 - l0. \quad (28)$$

Now we can change this value in final result, in corners Θ2, Θ3 calculation.

$$\Theta 2 = a\cos(\frac{(\sqrt{L^2+Y^2-S6^2*l4^2}-C234*l3-l0)*(l1+l2*C3)-(H-C234*C6*l4-S234*l3-h0)*S3*l2}{l1^2+l2^2+2*l1*l2*C3}), \quad (29)$$

$$\theta_3 = a\cos(\frac{(\sqrt{L^2+Y^2-S6^2*l4^2}-C234*l3-l0)^2+(H-C234*C6*l4-S234*l3-h0)^2-l1^2-l2^2}{2*l1*l2}). \quad (30)$$

Now we have calculated corners Θ1, Θ2, Θ3, without discontinuity points.

3. Conclusion

As result of calculation we have corners Θ1, Θ2, Θ3. Else corners are parameters of this equation, and can`t change in time of calculation. This result take possibility using corner Θ6 of grapple rotation. Corner Θ234 in calculation, is equal to corner between l3, and horizontal line. For robots with cornering part of arm l2, like on fig. 1 is need additional calculation of quadratic equation for Θ3. In this article for shorten calculation, l5=0mm.

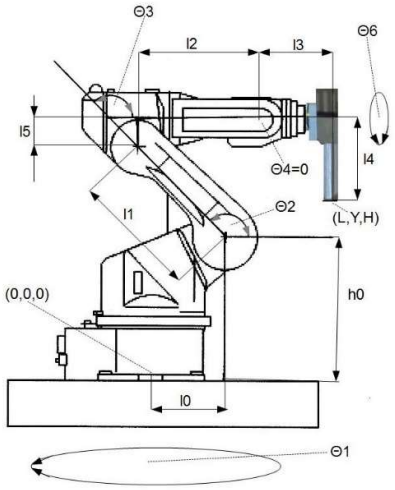

Figure 1. Producer outline scheme of robot Adept SX-300, with angles, and parts of robot arms.

Quality of this calculation is very high, and error of calculation is smaller to diameter of electron in hydrogen atom. So high quality making possibly using this equation, not only for apply for industrial robots, like Adept SX-300, but also to hi quality robots, working in very small raster, for example for microelectronic. Quality of this method, is very important for robotic producers, and for programming, and robotic scientist, designee special development for pharmacy, etc.

Annex: Specification of math symbols, and parameters of robot:

h0 – install height of robot arm over base,
l0 - horizontal displacement, to arm section l1, between Axis1, and Axis2,
l1 - length first arm section between points Axis2 and Axis3,
l2 - length second arm section of robot between points Axis3 and Axis5,
l3 - length third arm section between points Axis5 and Axis6,
l4 - length of grapple in vertical.
Θ1 – angle rotation around Axis1,
Θ2 – angle rotation around Axis2,
Θ3 – angle rotation around Axis3,
Θ4 – angle rotation around Axis5,
Θ6 – angle rotation around Axis6.
L – X coordinate point under grapple,
Y - Y coordinate point under grapple,
H - Z coordinate point under grapple.

References

1. Szkodny T.: Essentials of robotics. Gliwice: Silesian University of Technology publishing house, 2011.

SELECTED ENGINEERING PROBLEMS
NUMBER 7
INSTITUTE OF ENGINEERING PROCESSES AUTOMATION
AND INTEGRATED MANUFACTURING SYSTEMS

Grzegorz GOŁDA[1*], Adrian KAMPA[1]
[1] Institute of Engineering Processes Automation and Integrated Manufacturing Systems, The Faculty of Mechanical Engineering, Silesian University of Technology, Gliwice
[*]grzegorz.golda@polsl.pl

SIMULATION AND OFF-LINE PROGRAMMING OPTIMIZATION OF THE ROBOTIZED PRODUCTION CELL USING KAWASAKI K-ROSET SOFTWARE

Abstract: The article describes current researches realized during works on development of a new robotized production cell in Laboratory of Multimotion Control. Actual state of the station progress is shown. The study on optimization of off-line Kawasaki RS005L robot programming in AS-Language and virtual simulation with use of K-ROSET software are presented. At the end the further plans of the laboratory expansion and recommended researches are indicated.

1. Introduction

Modern solutions in automated and robotized, flexible manufacturing systems should give possibility of easy changes in manufacturing of products with different design and construction characteristics, but similar technology. This requires the use of computer simulation and off-line programming methods of every production equipment, like CNC technological machines, manipulation and transportation systems with robots and automated guided vehicles, even warehousing, because of fast reaction on the changes in future production (configuration, tools and programs for the cells, lines, departments, etc.) and quick response for a further, of course, clients orders [1]. In the newest Laboratory of Multimotion Control, the flexible, robotized cell with Kawasaki RS00L robot, is developed. During the expansion of the laboratory, a researches on off-line robot programming optimization, using different simulation techniques and software, are conducted [2,3,4]. The last study is connected with use of Kawasaki K-ROSET software included AS-Language programming interface [5,7].

2. Virtual simulation and off-line robot programming optimization

The effective robot and whole automated cell programming and its optimization require virtual simulation software, dedicated for real equipment. Only thus obtained, optimized operating parameters (robot trajectory without collisions, correct implemented logic and communications based on input/output signals, sequence and operation time of manipulation, production and other services) gives possibility to implement correct model in real production system and execution of planned tasks.

During the researches [3,5,6,7] on off-line programming optimization a virtual models of real robotized cells were created with use of the K-ROSET Lite 1.7.0 software. In a first step, the virtual models of robot tool adapter, gripper and other elements of created laboratory station (pallets, gravity conveyor, manipulation objects, stands and other constructions) were designed in CAD/CAE Siemens NX system and saved as a files with *.stl format, which is readable for the K-ROSET. After the choice of Kawasaki RS005L robot with correct control system E71, the import of CAD files (tools, work parts, equipments, obstacles) was necessary to map a real workstation environment. Identical (with reality) layout of objects, connection of robot gripper and configuration of virtual controller auxiliary data should be realized before off-line programming. The K-ROSET 3D simply model and expanded real station [5,7] are presented on Fig. 1.

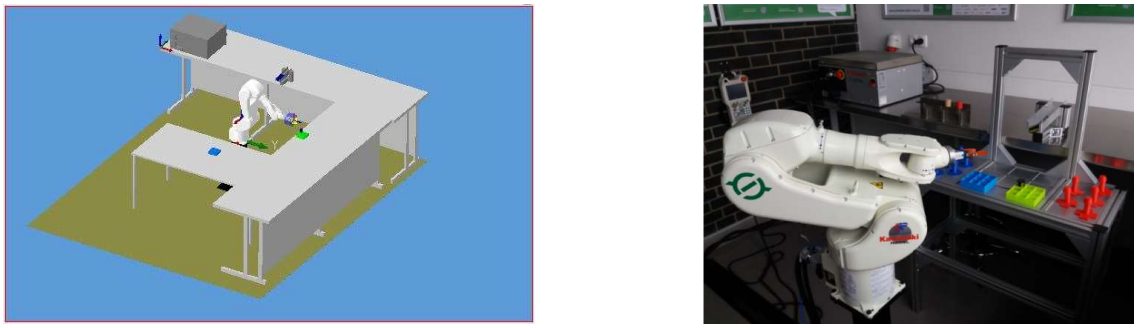

Fig. 1. The K-ROSET 3D simply model and expanded real laboratory station with Kawasaki RS005L robot

Next step was connected with creation of robot programs including block teaching (only for not complicated tasks and solutions - programs without optimization) and using AS-Language editor located inside virtual teach-pendant (programs to further optimization). First, it required the establishment of global and local program variables in K-ROSET (so-called "*real value*") concern with program loops, number of pallets, rows and columns etc., and position registers ("*joint value*" or "*trans value*"), which describe robot poses and transformations (e.g. robot or tool displacement in Joint, Base, Tool co-ordinate systems). All described data were entered to the system beyond the robot program, before and during programming.

Effective robot programming requires the use of large number of AS-Language instructions [8,9] relating to:

- definition of variables and calculation of robot's coordinates and positions - inside robot program:
  - "*variable / position instruction*": TOOL, BASE, HERE, POINT, DECOMPOSE, LLIMIT, ULIMIT,
- creation of collision-free trajectories:
  - "*motion instructions*": JMOVE, LMOVE, CMOVE, DRIVE, LAPRO, LDEPART, DRAW, SHIFT, TRANS, DELAY, HOME,
  - "*motion auxiliary instructions*": SPEED, ACCELERATION, DECELERATION, ACCURACY, PAUSE, TIMER, BREAK,
- connected with realization of other tasks and operations, not related with robot movement :

- "*input / output instructions*": OPEN, CLOSE, SIGNAL, PULSE, BITS, SWAIT, TWAIT, RESET,
- "*program control instructions*": CALL, GOTO, IF, THEN, ELSE, ON, FOR, END.

After robotized cell programming in AS-Language, the optimization of created solutions was conducted. The elimination of unnecessary points of robot or tool trajectory (minimization of unproductive kinematic chain movements while maintaining the collisions-free paths) and reduction of redundant program instructions (by the use of logic and program control instructions for creating robot macros for typical applications, instead of block teaching) were the main optimization criterions.

The method of off-line programming, sample program optimization and virtual visualization and simulation in K-ROSET software are presented on the Fig. 2.

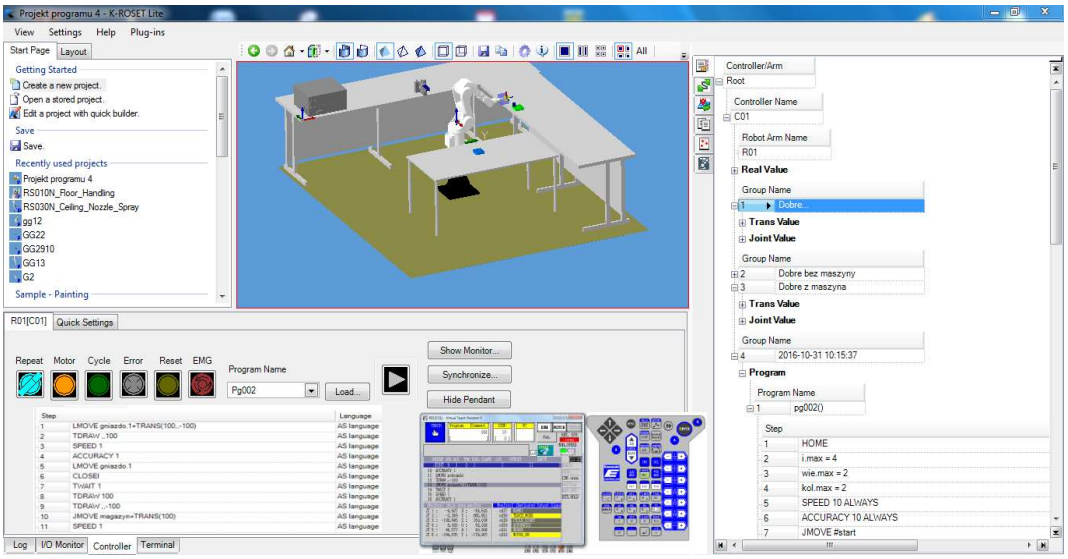

Fig. 2. Off-line programming, program optimization and virtual simulation of robotized cell using the K-ROSET Lite 1.7.0 software

The main aim of realized researches and off-line optimizations was improving the performance and productivity of robotized cell, and speed up process of Kawasaki robots off-line programming by creating user defined subprograms and macros for typical or untypical solutions (manipulation, palletizing, machining, rapid prototyping and other).

Parallel to the works and researches on off-line programming and optimization, the real components of robotized cell were fabricated. Some of them (gripper clamps, pallets) were produced using modern 3D printing rapid prototyping method. Other equipment was manufactured by classical machining methods. Some dimensional problems connected with precision of fabricated elements can occur. Therefore, the main problem with correct robot calibration, can be associated with the reference point of scene coordinate system.

Off-line created and optimized, in the terms of accepted criteria, programs were uploaded into robot control system and tested successfully, according with the safety principles, on the laboratory station.

3. Future works, researches and conclusion

Further works on the development of the laboratory station with Kawasaki RS005L robot require its expansion of other components like: robot tools (double gripper, vacuum surface gripper, automated tool's changer, spot welding and painting simulator, milling tool or 3D printer etc.), external equipment (external I/O and vision system, CNC machines and warehouses, safety system) and other robots. It is necessary to do future researches on programming and optimization of multi-robots cells for standard (e.g. spot welding, painting) and atypical (e.g. rapid prototyping and multi-tool machining) solutions.

Data obtained during Kawasaki robot off-line programming and K-ROSET modeling will be used in product lifecycle management class simulation software (PLM) and in software for production and logistic flow optimization (e.g. Enterprise Dynamics 8, Flexsim 7, etc.). It gives possibility of creation effective enterprise production and logistic system before its real implementation and later allows to optimize the performance of the structure and realized processes. This is consistent with progress towards digital manufacturing.

References

1. Shivanand H., Benal M., Koti V.: Flexible manufacturing system. ISBN: 978-81-224-1870-5, UVCE, Bangalore, Karnataka 2006.
2. Gołda G., Kampa A.: A micrologistics system analysis on example of robotized rapid prototyping cell. Selected Engineering Problems vol. 5, Gliwice 2014, pp. 37-40.
3. Gołda G., Kampa A., Paprocka I.: The application of virtual reality systems as a support of digital manufacturing and logistics. IOP Conference Series: Materials Science and Engineering. vol. 145-042017, doi:10.1088/1757-899X/145/4/042017, 2016,
(http://iopscience.iop.org/article/10.1088/1757-899X/145/4/042017/pdf, access: 23.09.2016).
4. Sękala A., Gwiazda A., Foit K., Banaś W., Hryniewicz P., Kost G: Agent-based models in robotized manufacturing cells designing. IOP Conference Series: Materials Science and Engineering. vol. 95-012106, doi:10.1088/1757-899X/95/1/012106, 2015,
(http://iopscience.iop.org/article/10.1088/1757-899X/95/1/012106/pdf, access: 10.01.2016).
5. Pawlaczyk T.: The development of laboratory and programming the Kawasaki robot in AS language. Master thesis (realized under the direction of supervisor: dr. eng. Grzegorz Gołda), Gliwice, 2016.
6. Kampa A., Gołda G.: Rapid machining with industrial robot. Selected Engineering Problems nr 5, Gliwice 2014, s. 57-62.
7. Students' Science Club of the Design and Exploitation of Robotized Systems - unpublished researches on the flexible manufacturing systems modeling, simulation and robots off-line programming (realized under the direction of supervisor: dr. eng. Grzegorz Gołda), Gliwice, 2016.
8. Kawasaki Robotics GmbH. K-ROSET – Technical documentation, tutorial and help of the software, 2015.
9. Astor Sp. z o.o.: Utility software: K-ROSET - product and software description,
(https://www.astor.com.pl/produkty/robotyzacja/oprogramowanie-narzedziowe/k-roset.html, access: 20.02.2016).

SELECTED ENGINEERING PROBLEMS
NUMBER7
INSTITUTE OF ENGINEERING PROCESSES AUTOMATION
AND INTEGRATED MANUFACTURING SYSTEMS

Adrian KAMPA[1*], Grzegorz GOŁDA[1]
[1] Institute of Engineering Processes Automation and Integrated Manufacturing Systems,
The Faculty of Mechanical Engineering, Silesian University of Technology, Gliwice, Poland
[*]adrian.kampa@polsl.pl

COMPUTER AIDED DESIGN OF HUMAN WORKSPACE AND MANUALLY OPERATED PROCESSES

Abstract: The design of human workspace and manually operated processes can be improved with the use of digital models of human body. An example of design human workspace in CAD software NX 10 and simulation example of work process in Jack software are presented. The use of digital human models allows to improve the ergonomics of human workspace and simulation of work process can be used for calculation of standard work time.

1. Introduction

The design of workspaces and manufacturing processes is a multi-stage process requiring solutions of problems from many fields. It includes both technical problems as well as ergonomics and work safety. Despite the increasing automation and robotization of manufacturing, human labor is still required. This applies in particular to the assembly processes and processes requiring the participation of skilled workers. This is due to the fact that people have innate manipulation skills and easily learn new activities.

An important step is conceptual design which access to detailed design. In traditional design, a two-dimensional drawings and sketches, which do not reflect the full spatial picture of the situation in the workplace, are used. The human body has some limitations and therefore is essential to adapt the workspace for the possibilities of the human body. This includes, inter alia, proper body position, the range of hands, field of view, and distance from dangerous places. Therefore, the use of three-dimensional digital models of the human body for a full visualization of the spatial position in CAD system is preferred [1].

Computer modeling of the human body dates from the 1970s. Initially, these models were very simplified, but they have been improved gradually, so as to fully map the parameters of the human body. Currently there are a number of digital human models available, such as, AnyBody, Delmia Safework, HumanCAD, JACK, ManneQuinPRO, Sammie [2, 4, 6, 10]. They are parameterized and based on anthropometric databases such as ANSUR, NHANES, and can be used in many CAD systems [2].

2. Manually operated processes

The second important type of human behavior modeling, which concentrates on predicting the perceptual-cognitive aspects of human performance. Models of this type have been referred to as human performance process models. The primary motivation for the development of these models has been to understand and predict the time required for different people to perform a task without errors, especially when the task has a high perceptual and/or cognitive load [2].

A contemporary example of this would be when a worker is manually operating a complicated machinery. Accurately predicting under what specific conditions a person would be able to control the machine safely is of immense importance, especially when designing or specifying various types of human-machine interface, such as visual displays, automatic safety systems, and night vision systems.

In industrial engineering, the standard time is the time required by an average skilled operator, working at a normal pace, to perform a specified task using a prescribed method [3]. It includes appropriate allowances to allow the person to recover from fatigue The usage of the standard time are very important and therefore some different method are used for standard time calculation [7].

The one of the most used method in industrial engineering is MTM (Methods-Time Measurement). MTM is a predetermined motion time system that is used primarily in industrial settings to analyze the methods used to perform any manual operation or task and, as a product of that analysis, set the standard time in which a worker should complete that task. The essence of this system is that the individual work activities are spread out into smaller units of movement. In the basic method of MTM-1, these are 17 basic movements. In general there are 5 moves mainly used. These movements include: reaching, grasping, moving, pressing, release. The individual movements are evaluated on the basis of the tables with normative activity time. From these analyses, work standard times are derived. Proper use of the MTM method require very good knowledge about work process in order to obtain correct results.

3. Digital human modelling

Ergonomic work requires sitting or standing body position. Workspace height should be a prime consideration. General work can be done at the normal height of about 900 millimeters. During precision work, the height should be raised to prevent straining of the back, neck, and shoulders. Seating the body in order to bring the workspace closer to the worker is a common solution. Adjustable height workbenches are also available in some cases [8, 9].

An example of digital human model from NX CAD software is presented in the figure 1. The human model with typical body structure was selected with 1750 mm height. It is based on ANSUR anthropometric database. That model is fully scalable and has movable joints. This enables to move each part of body and get different poses.

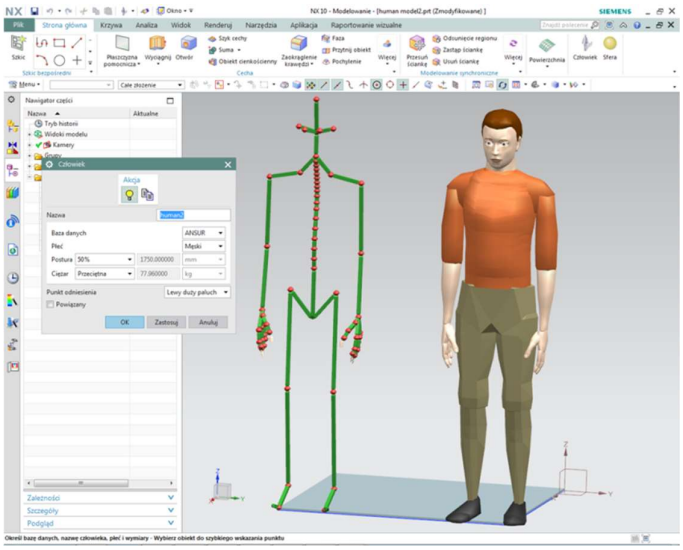

Fig. 1. Digital model of human body and skeleton in NX 10 software

The digital human model was then used for workspace design. The example of human worker operating a machine is presented in the figure 2. We can see that this machine is too low for ergonomic work. That situation can result in work-related musculoskeletal disorders (WRMDs) connected with persistent pain, loss of functional capacity and work disability [8].

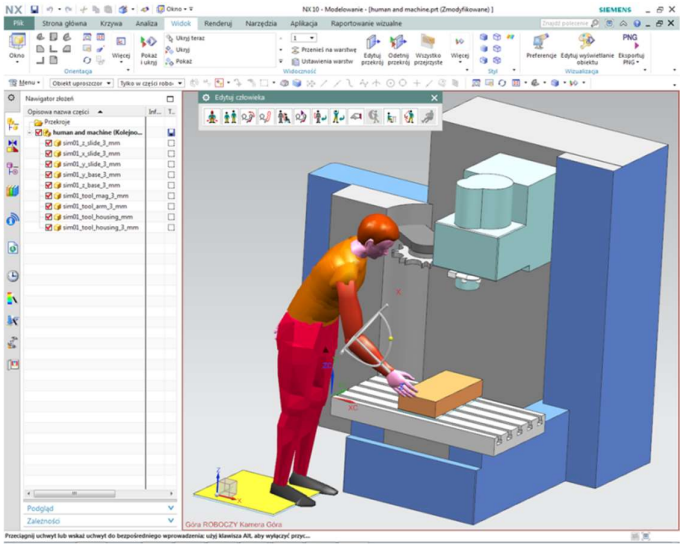

Fig. 2. 3D workspace view of human operating the machine

However detailed analysis of human work process was made with another software tool.

4. Simulation of human work process

Human work requires many movement activities. Jack software, which is a human modeling and simulation tool, was used for modeling and simulation of human work. Jack human model is made up

of 71 segments, 69 joints and 135 degrees of freedom [5]. An example of human model creation is shown in the figure 3.

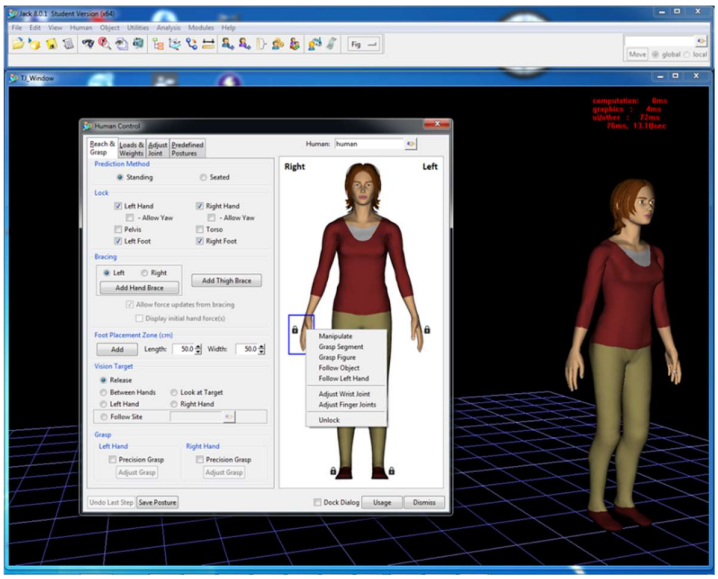

Fig. 3. Example of human model in Jack software

Jack enables improvement of the ergonomics of your designs and to refine industrial tasks. Also provides human-centered design tools for performing ergonomic analysis of virtual products and virtual work environments. Jack enables you to size your human models to match worker populations, as well as test your designs for multiple factors, including injury risk, user comfort, reachability, line of sight, energy expenditure, fatigue limits and other important human parameters [6].

Another example include work process from industrial practice that require manipulation with rectangular box and transport it from machine to conveyor (fig. 4).

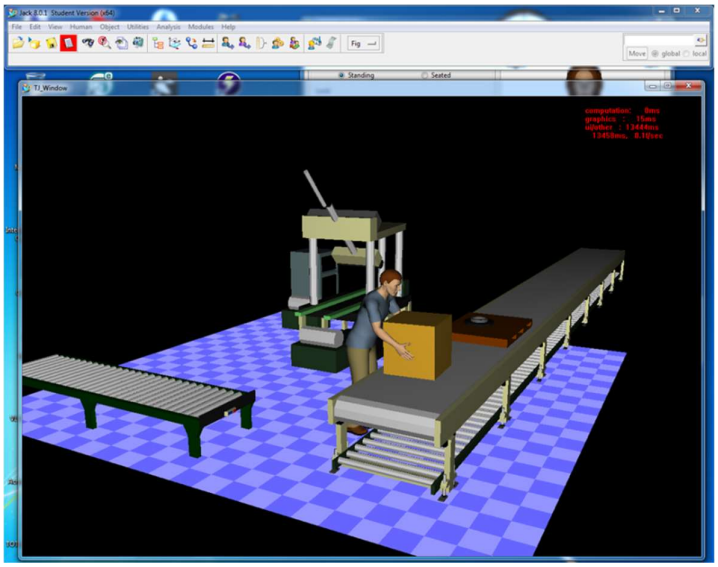

Fig. 4. Example of transport task in Jack software

Next simulation of worker movement activities was conducted. One of the simulation step is presented in the figure 5.

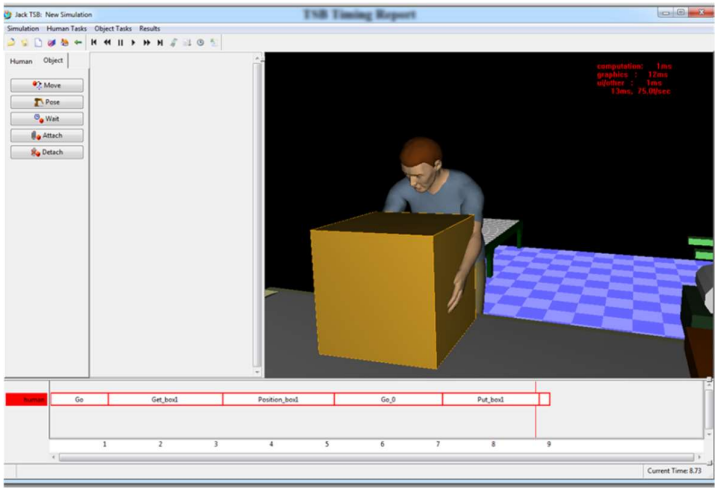

Fig. 5. Simulation of transport task in Jack software

As a result from simulation a human task summary was acquired (Tab. 1), which contain the same action description as is in the MTM method.

Table 1. Simulation report of human activity

Task Summary human			
Task	*Action*	*Duration*	*Code*
Go		**1.04**	
	Walk	1.04	W3FT
Get_box1		**2.06**	
	Bend_And_Reach	1.99	B + R20.704A(b)
	Grasp	0.07	G1A(b)
Position_box1		**2.01**	
	Arise_And_Reach	2.01	AB + R18.356A(b)
Go_0		**1.95**	
	Walk	1.95	W5FT
Put_box1		**1.75**	
	Bend_And_Reach	1.67	B + R11.727A(b)
	Release	0.07	RL1(b)
Go_1		**0.19**	
	Walk	0.19	W0FT

The simulation allows to verify the results obtained from MTM method and more precise calculation of standard work time.

5. Conclusion

Ergonomic workspace design is very important for human health. The technology of digital human modelling has the potential to drastically change and improve the process by which most designers decide on the appropriate human physical attributes to consider in a workspace when attempting to meet ergonomics and production goals. In addition digital simulation of human work process enables prediction of time required for different people to perform a task. Using digital human models facilitates significant cost and time savings by enabling product quality improvement and process feasibility, early in the product lifecycle.

References

1. Chaffin D. B.: Digital Human Modeling for Workspace Design. Reviews of Human Factors and Ergonomics October 2008 vol. 4 no. 1 41-74, doi: 10.1518/155723408X342844.
2. Duffy V. G. (ed.): Handbook of Digital Human Modeling: Research for Applied Ergonomics and Human Factors Engineering. CRC Press, London, 2016.
3. Groover, M. P.: Work systems: the methods, measurement and management of work, Prentice Hall, 2007.
4. Human Modelling Software. http://www.nexgenergo.com/ergonomics/ergoprods.html
5. Jack User Manual Version 8.0.1. Siemens Product Lifecycle Management Software Inc., 2013.
6. Jack and Process Simulate Human: https://www.plm.automation.siemens.com/pl pl/products/tecnomatix/manufacturing-simulation/human-ergonomics/jack.shtml#lightview-close.
7. Karger D. W., Bayha, F. H. Engineered Work Measurement. Industrial Press, New York, 1987.
8. Karwowski W. (Ed.): International Encyclopedia of Ergonomics and Human Factors, CRC Taylor & Francis, 2006.
9. Projektowanie miejsc pracy. Postępowanie metody i wiedza techniczna. CIOP, Warszawa 2002.
10. The SAMMIE DHM System http://www.lboro.ac.uk/microsites/lds/sammie/dhm.html.

SELECTED ENGINEERING PROBLEMS
NUMBER 7
INSTITUTE OF ENGINEERING PROCESSES AUTOMATION
AND INTEGRATED MANUFACTURING SYSTEMS

Klaudiusz KLARECKI*

Institute Of Engineering Processes Automation And Integrated Manufacturing Systems, Faculty of Mechanical Engineering, Silesian University of Technology, Gliwice
*klaudiusz.klarecki@polsl.pl

THE IMPACT OF THE FILTRATION PARAMETERS FOR HYDRAULIC FLUIDS CONTAMINATION

Abstract: The article is focused on the filtration phenomena of hydraulic fluids. It describes the mathematical model of this phenomenon. It has been shown that the appropriate selection filtration in the hydraulic system requires not only the proper properties of the hydraulic filter. Just as important are:
- Flow rate through the filter.
- The value of particulates flux causing an increase in contamination of hydraulic fluid.

1. Introduction

Frequent opinions is that hydraulic drives are very unreliable. Most often the users themselves contribute to a hydraulics failure. According to the manufacturers of hydraulic components, more than 70% of failures are caused by dirty hydraulic fluids. It is worth asking if the hydraulic users are like naughty children and they destroy purposely their hydraulic drives? Maybe the problem of hydraulic fluid contamination depends not only on the user's procedures.

2. Filters and filtration

Pure hydraulic fluid starts with the design of hydraulic circuit. It involves the proper selection of filter and its appropriate arrangement in the circuit.

Into hydraulic drives usually mechanical filters are used. Mechanical filters are divided into:
- surface filters,
- depth filters.

The advantage of the surface type filter is that it can be regenerated. Depth type filters can collect more contamination particles (dirt holding capacity of depth filters are much more higher than surface filters), so its life time is significantly higher.

Suction strainers and fillers are type surface filters. Pressure line filters and return line filters are mainly depth type.

Typical mounting places for filters are:
- suction line,

- pressure line,
- return line,
- kidney-loop (off-line filtration).

Occasionally, hydraulic filters are installed in several places of hydraulic circuit. Pressure line filters are installed onto inlets of components which are sensitive to contamination to protect them. Besides, hydraulic circuit is equiped with a main return line filter or off-line filter. This is very effective but expensive solution of filtration.

The main features of hydraulic filter are:

- nominal flow,
- pressure losses,
- dirt holding capacity,
- Beta ratio.

Beta ratio $\boldsymbol{\beta_x}$ is a formula used to calculate the filtration efficiency of a particular fluid filter using base data obtained from multi-pass testing (Fig. 1). The formula used to calculate $\boldsymbol{\beta_x}$ is:

$$\beta_x = \frac{N_u}{N_d} \tag{1}$$

whereby:

N_u – particle count in upstream fluid,
N_g – particle count in downstream fluid,
x – particle size.

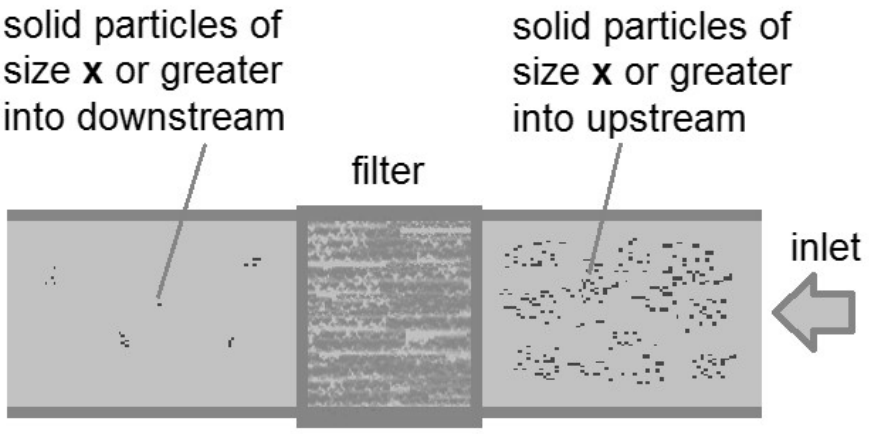

Fig. 1. Multi-pass testing

Particulate removal efficiency $\mathbf{n_f}$ can be seen as the probability of capturing particles flowing through the filter. The relationship between beta ratio and nf is given by the formula:

$$n_f = \left(1 - \frac{1}{\beta_x}\right) \cdot 100\% \tag{2}$$

3. Analysis of the impact of selected filtration parameters on the cleanliness of hydraulic fluid

For the analysis it has been adopted most common arrangement - with return line filter (Fig. 2).

Initially it was assumed that the cleanliness of the hydraulic fluid depend on the:
- filter efficiency,
- actual filter flow rate,
- tank volume.

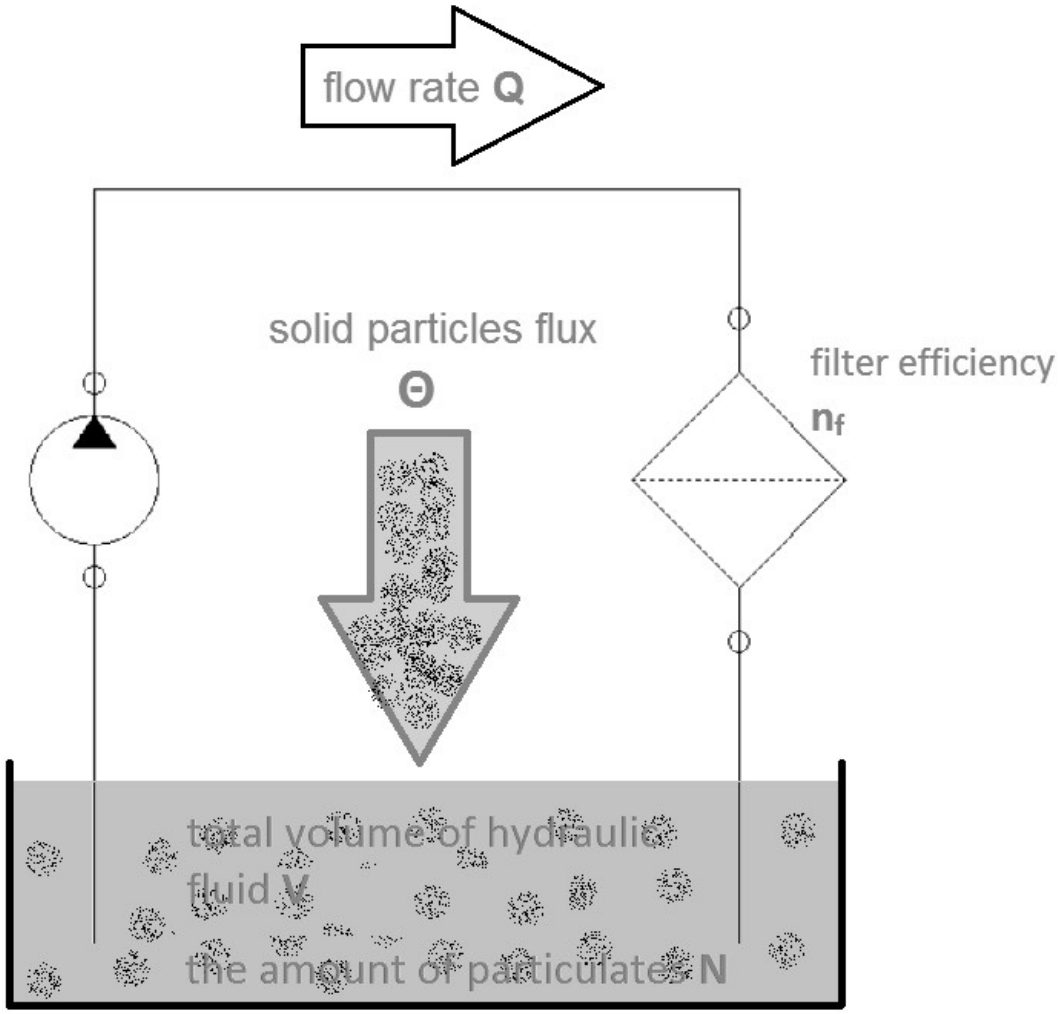

Fig. 2. Sketch of the analyzed hydraulic system

Model of filtration phenomena

Model of filtration phenomena was based on the following assumptions:
- filter efficiency is equal the probability of capturing particles with size x or greater,
- particulates are evenly distributed in the liquid,

- the inner and outer particulates with total flux Θ enters the hydraulic liquid, particulate flux is accepted as constant,
- particulates appear uniformly throughout the entire volume of hydraulic fluid.

The probability of capture contaminant particle over unit time **λ** can be accept as:

$$\lambda = \frac{n_f}{100\%} \cdot \frac{Q}{V} \tag{3}$$

Whereby:

Q – flow rate through filter,

V – total volume of hydraulic fluid into circuit.

Assuming a small value of λ, the formula for the number of dirt particles N in the hydraulic fluid can be written as follows:

$$\frac{dN}{dt} = -\lambda N + \Theta \tag{4}$$

Whereby:

Θ – solid particulates flux

It can be seen that formula (4) is same to describing the phenomenon of radioactive decay.

Combining (3) and (4) were obtained:

$$\frac{dN}{dt} = -\frac{n_f}{100\%} \cdot \frac{Q}{V} N + \Theta \tag{5}$$

In general, the factors that determine the number of particles of pollutants according to (5), are not fixed. For example, filtration efficiency may depend on the degree of filling of the filter. Also, the liquid volume in the system may be varied, e.g. due to leakages.

Determination of the number of pollutants, taking into account the variability of factors $\mathbf{n_f}$, **Q**, **V** and **Θ** most likely require the use of numerical methods to solve the equation (5). Further analysis was accepted a simplified model of filtration phenomenon in which factors have fixed values. According to the accepted simplification, the solution of equation (5) is particular integral in a particular as a:

$$N = N_0 e^{-\frac{n_f}{100\%} \cdot \frac{Q}{V} t} + \Theta \frac{V \cdot 100\%}{n_f \cdot Q} \left(1 - e^{-\frac{n_f}{100\%} \cdot \frac{Q}{V} t} \right) \tag{6}$$

Whereby:

ρ_{c0} – initial concentration of particulates.

For formulas (6) and (7) can enter the time constant filtration $\mathbf{T_f}$ as:

$$T_f = \frac{V \cdot 100\%}{n_f \cdot Q} \tag{8}$$

It should be noted that for the filtration times t >> T_f , the concentration of particulates approaching the values:

$$\rho_c = \frac{\Theta \cdot 100\%}{n_f \cdot Q} \tag{9}$$

From (9) it follows that for a given flux of particulates **Θ**, the particle concentration can be reduced by increasing filter efficiency $\mathbf{n_f}$ or increasing the flow through the filter **Q**.

Which way is more efficient? It will be analyzed in the example 1.

Example 1

Compare two hydraulic systems with 1000 dm^3 volume of hydraulic oil. First is equipped with a return line filter with $\beta_{10\mu m} = 300$. The off-line filtration with $\beta_{3\mu m} = 75$ filter is applied to second unit. Both systems work 24/7 in same environment with Θ = 1E+7 [1/s] flux of particles size 4 μm and above. Flowrate of main pump is 200 dm^3/min, flowrate of auxiliary pump is 50 dm^3/min (second unit). Initial fluid contamination was accepted as upper range of class 22 according ISO 4406.

Based on the item [2] were calculated beta ratios for particles with a size 4 microns. Beta ratio of filter with $\beta_{10\mu m} = 300$ was calculated 10, and for filter with $\beta_{3\mu m} = 75$ its beta ratio was 200. So the efficiencies of capture particles ≥ 4 microns are as follows:

- $n_{f1} = 90\%$
- $n_{f2} = 99{,}5\%$

The calculation results for Example 1 in accordance with formula (7) shown in Fig. 3.

Obtained results prove that the contamination of hydraulic fluid strongly depend on filter flow rate.

The calculated values of the particulates concentration in the steady state are as follows:

- return filter - $\rho = 3.33 \cdot 10^5$ particles / 100 ml,
- off-line filter - $\rho = 1.21 \cdot 10^6$ particles / 100 ml

For return line filter with $\beta_{10\mu m} = 300$ user can expect 19/.../... ISO cleanliness code (250.000 ÷ 500.000 range of particles number per 100 ml) . But for the off-line filtration with $\beta_{3\mu m} = 75$ probably value of ISO cleanliness code will be 21/…/… (1.000.000 ÷ 2.000.000 range of particles number per 100 ml).

It should be noted that in both filtration methods the cleanliness of hydraulic fluids is not met to ensure ISO class 18/16/13.

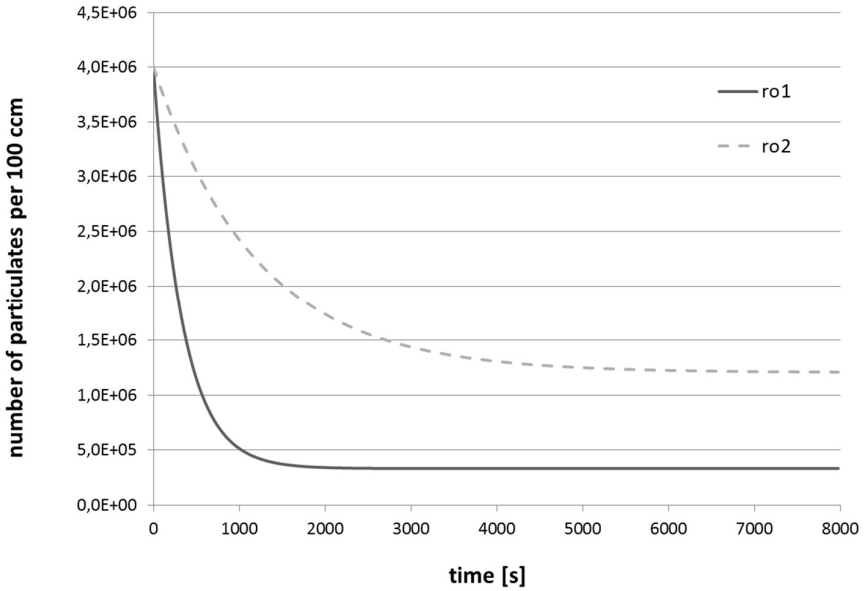

Fig. 3. The course of particulate concentration of pollutants of hydraulic systems from example 1

4. Conclusion

The considerations about the phenomenon of filtration in hydraulic systems were based on a model based on several simplifying assumptions, so that is possible get its analytical solution. A more adequate researches of filtration processes probably will require the adoption of numerical models and carrying out a series of experimental studies.

Thanks using analytical method was obtained proof of strongly relationship between filter flow rate and cleanliness of hydraulic fluid.

The calculation results indicate the importance of the knowledge of the particulates flux for proper design of filtration in a hydraulic system. Increasing the filter Beta Ratio does not bring significant changes of the cleanliness of the hydraulic medium. The results should not be interpreted as meaning that for hydraulic units are sufficient filters for higher particulate sizes "x".

The filters with acceptable Beta Ratio for particulates with high sizes ("x" above 10 microns) can't prevent hydraulic units from dust particles (with a size less than 4 microns), which can lead to accumulating of sediments into hydraulic elements.

A large amount of dust particles is causing the failures of valves and accelerated wear of cooperating parts. It also leads to accelerated degradation of the hydraulic fluid, and can promote the cavitation.

References

1. Tomasiak E.: Napędy i sterowania hydrauliczne i pneumatyczne. Wydawnictwo Politechniki Śląskiej, Gliwice 2001.
2. HYDAC Filtration Handbook no E70.000.0/02.08 www.hydac.com.au (01.08.2016).

SELECTED ENGINEERING PROBLEMS
NUMBER 7
INSTITUTE OF ENGINEERING PROCESSES AUTOMATION
AND INTEGRATED MANUFACTURING SYSTEMS

Klaudiusz KLARECKI[1*], Dominik RABSZTYN[2]

[1,2]Institute of Engineering Processes Automation and Integrated Manufacturing Systems,
Faculty of Mechanical Engineering, Gliwice, Poland
[*]klaudiusz.klarecki@polsl.pl

INFLUENCE OF THE DRIVE WITH FREQUENCY INVERTER ON PRESSURE PULSATION OF A GEAR PUMP

Abstract: The article presents the results of preliminary experimental tests focused on pressure pulsations of gear pump type PGP511 with the inverter-fed drive. The obtained results were compared with the pressure pulsation of the examined gear pump powered in a conventional way. A cycle of measurements was carried out for variable hydraulic resistance and fixed temperature of hydraulic fluid. The obtained results were analyzed in time and frequency domains.

1. Introduction

Development of modern hydrostatic systems is not connected only with increasing density of the transmitted power and enhancing efficiency of the selected elements of the hydraulic system, but it also comprises reducing vibration and noise levels (with mechanical or hydraulic sources) [6, 10]. Vibration resulting from pressure pulsation, caused by the irregular flow rate (pressure pulsation) of the system's hydraulic fluid, causes the accelerated wear of working parts, reduces accuracy of positioning the receivers and increases emission of noise. Therefore, it is necessary to conduct research aiming at the analysis of phenomena influencing pressure pulsation on the discharge line. [2, 3, 4].

We may observe a tendency to replace traditional solutions, in stationary hydraulic systems with variable displacement pumps, with a mechatronic equivalent with the similar functionality [1, 8, 9]. A hydraulic power unit that is based on this concept most commonly features a fixed displacement pump powered by electric motor with infinitely adjustable rotational speed. Drive system of a displacement pump with infinitely adjustable rotational speed enables setting pump's flow rate in a way allowing for obtaining the desired speed of the hydraulic receiver. Thereby, we obtain a hydraulic system with volumetric control that is characterized by the improved performance as compared to hydraulic units with throttle control. [5, 7].

This article, however, focuses on a certain danger connected with using frequency inverters. Authors of the publication pose the following question: is transferring harmonic distortion on pumping pressure pulsation possible for the drive with frequency inverter?
The obtained pumping pressure pulsation curves were analyzed in time and frequency domains. Time domain analysis was carried out in order to determine peak-to-peak value

of pumping pressure that influences fatigue wear of the hydraulic system components and is responsible for generating increased levels of vibration and noise. Frequency domain analysis was carried out in order to identify the differences between frequency responses in case of the examined gear pump powered either by the motor with frequency inverter or with the same motor with direct electric power supply.

2. Measuring station and experiment plan

A measuring system (Fig. 1) has been composed of a gear pump with external gear design (series PGP511 produced by Parker Hannifin) with the capacity of 8cm^3, powered by asynchronous AC motor was fed by the Parker Hannifin AC10 frequency inverter and conventionally (direct electric power supply) and a throttle valve 9N600S (regulation of hydraulic resistance). A pressure sensor HDA 4748-H-0250 was mounted at the discharge flange of the pump. Working fluid temperature (mineral oil HLP46 class) during the experiment was 40°C. Results of the experiment were acquired using HYDAC HMG3010 measuring and data-acquisition device.

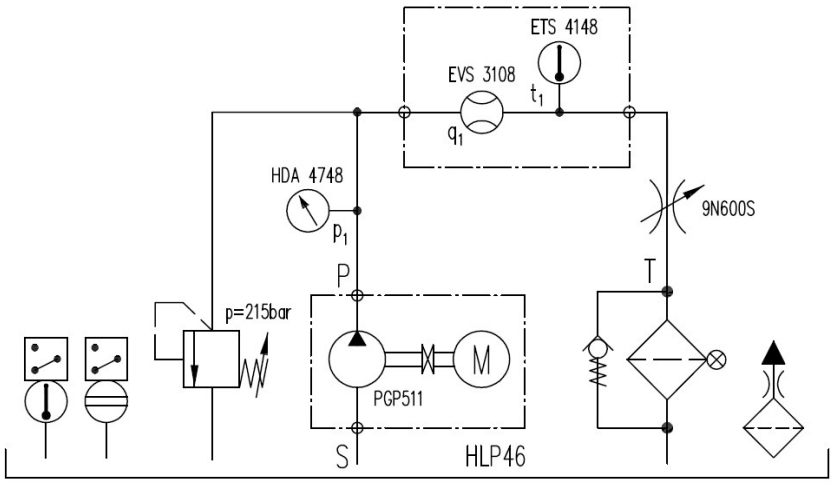

Fig. 1. Simplified hydraulic diagram of a measuring station

Measurements were carried out according to table 1. The tests were conducted for the system with conventional drive with asynchronous motor powered by inverter. Variable parameters included pressure in the pressure line at the constant temperature of the working fluid (t=40°C, HLP46 oil) and fixed electric grid frequency. The pressure was set by assuming hydraulic resistance of the pressure line by opening of the throttle valve.

Table 1. Experiment plan

No.	Test symbol	Pressure in the pressure line [bar]	Frequency of motor current [Hz]	Inverter drive system
1	PC_50	50	50	No
2	PC_100	100		
3	PC_150	150		
4	PF_50	50		Yes
5	PF_100	100		
6	PF_150	150		

Frequency of sampling signals registered during the experiment was 10kHz. Peak-to-peak pressure value was determined over the 100ms time interval. 16384 samples analyzed in the rectangular window were taken for the FFT-based data processing.

3. A comparative analysis of pump pulsation with inverter drive and with direct electric power supply

Selected comparative results of pumping pressure pulsation for the conventional drive system of a gear pump and a inverter drive are presented in table 2.

Table 1. Selected results of experimental tests

No.	Test symbol	Pressure in the pressure line [bar]	Time domain			Frequency domain	
			p_{max} [bar]	p_{min} [bar]	Δp [bar]	p_n for 25Hz [bar]	p_p for 300Hz [bar]
1	PC_50	50	49,5	50,4	0,9	0,057	0,32
2	PC_100	100	99,3	100,5	1,2	0,096	0,374
3	PC_150	150	149,7	150,9	1,2	0,128	0,276
4	PF_50	50	20,2	51,1	0,96	0,07	0,256
5	PF_100	100	99,5	101,1	1,6	0,122	0,331
6	PF_150	150	149,9	151,4	1,5	0,144	0,345

Basic experiments aiming at comparing gear pump drives are PC_100 and PF_100 according to table 1, whose pressure spectrums are presented in fig. 4 and 5.
Pressure pulsation spectrums presented in fig. 2 and 3 are similar. In both, we may observe a dominant band spectrum correspondent to the frequency of teeth engagement f_p. Amplitude of pressure pulsation for this frequency is 0,374bar with power supply direct from the network and 0,331bar with inverter drive. We may assume that using the inverter slightly (by about

11,5%) improved pressure pulsation for the dominant frequency. Another positive aspect of the inverter drive is eliminating pressure pulsation for the first harmonic frequency of pump shaft rotation $2*f_n = 50Hz$. On the other hand, within the range of low frequencies we may observe their higher amplitudes for the pump powered by the inverter.

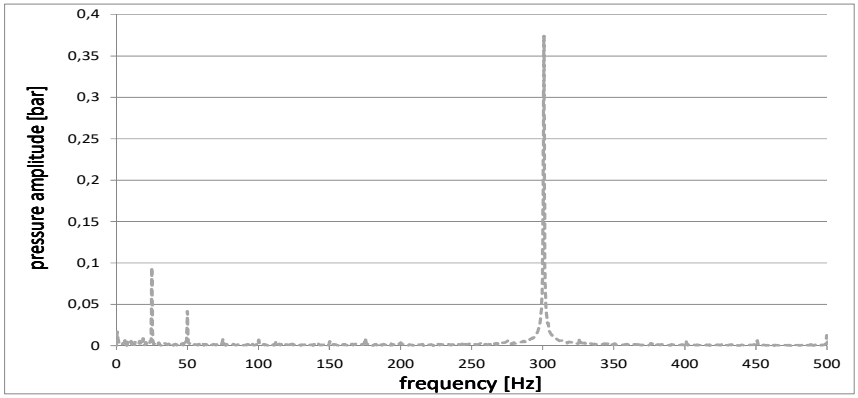

Fig. 2. Pressure pulsation spectrum for experiment PC_100 (without inverter)

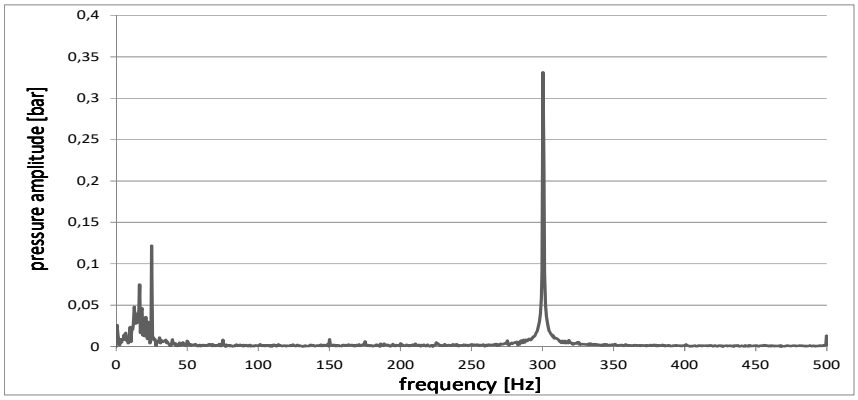

Fig. 3. Pressure pulsation spectrum for experiment PF_100 (with inverter)

For the purposes of more accurate comparison, fig. 4 presents both spectrums within the range up to 100Hz. It may be noticed that pressure pulsation for the frequency of pump shaft rotation f_n is 29% greater in case of the inverter drive.

Additionally, a blurred pressure pulsation band spectrum with maximum for the frequency 16,5Hz was observed in the pressure pulsation spectrum of a pump powered by the motor with inverter. It is quite unfavorable due to the possibility of evoking the response of a pressure line in a wider range of low frequencies that may overlap the line's natural frequencies in lengths of meters.

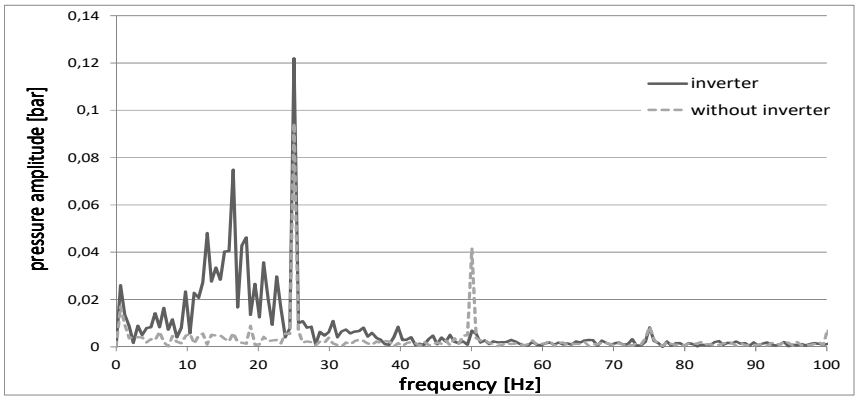

Fig. 4. Pressure pulsation spectrum for experiments PC_100 i PF_100

In order to confirm or deny the differences in the operation of a gear pump depending on its drive system, we have repeated the tests for pumping pressures 50bar and 150bar. Fig. 5 demonstrates spectrums for both drives with average pumping pressure 50 bar; analogical spectrums obtained for the average pumping pressure 150bar are presented in fig. 6.

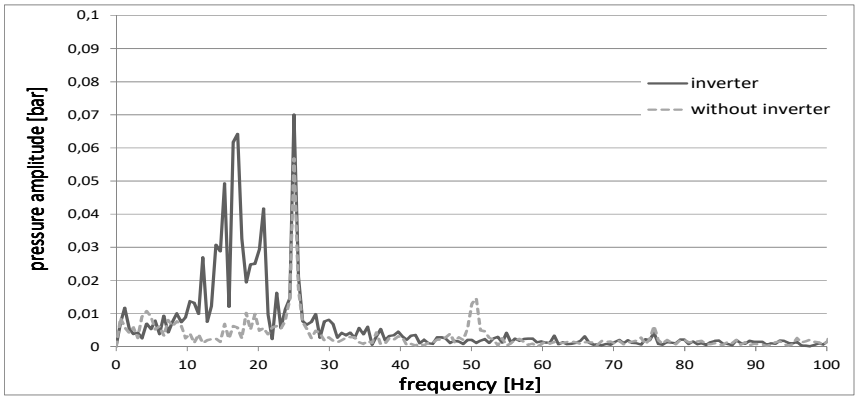

Fig. 5. Pressure pulsation spectrum for pumping pressure 50 bar

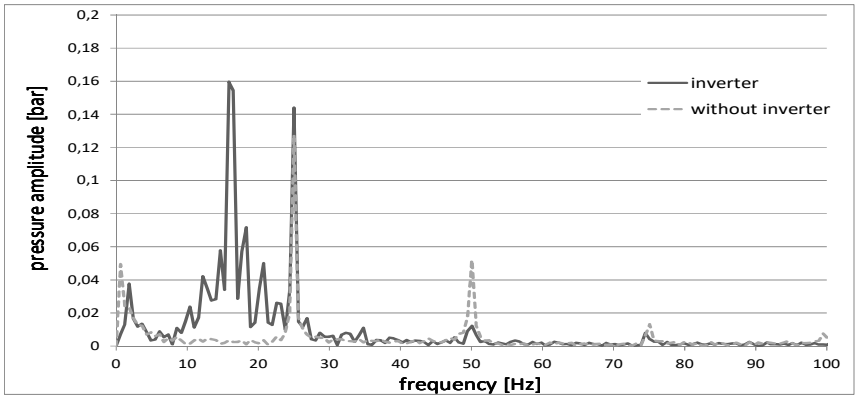

Fig. 6. Pressure pulsation spectrum for pumping pressure 150 bar

Results shown in fig. 5 and 6 are very similar to the spectrums obtained in experiments PC_100 and PF_100. Therefore, it may be assumed that it is a characteristic feature for the examined pump with inverter drive to demonstrate pressure pulsation within the frequency range between 12Hz to 20Hz. It may also be observed that the maximum value of this pulsation, occurring at about 16,5Hz, depends on the average pumping pressure (from 0,064bar at minimum value of average pressure to 0,16bar at its maximum value). These figures are proper for nominal rotational speed of pump's motor.

4. Conclusion

Results of the research indicate that there is a dependency between drive type of a gear pump and pumping pressure pulsation. It is, however, hard to conclude that this is an unambiguously negative influence. The obtained results proved that within the range of lower pumping pressure, pressure pulsation for the dominant frequency f_p was lower in case of the inverter drive. Furthermore, with this drive type, we did not observe the band spectrums of the first harmonic frequency of pump shaft rotation. The undoubted disadvantage of the inverter drive for gear pump PGP511 is the occurrence of blurred band spectrums of pressure pulsation in the range of low frequencies. A thorough examination of the causes of this phenomenon would require constructing a new research unit enabling measuring torque on the motor shaft and electrical values at its power supply provided by the inverter.

Additionally, another undesirable feature of the inverter drive is a noticeable increase of pressure pulsation amplitude at the frequency of pump shaft rotation.

In conclusion, it must be noted that hydraulic power units equipped with inverter should be examined by the interdisciplinary team of researchers in terms of their electrical, mechanical and hydraulic properties.

References

1. Gozdalik M.: Hydraulic device with constant pump and variable electric motor. Hydraulic and Pneumatic, Nr 1/209, pp. 5-11 (in Polish).
2. Klarecki K., Rabsztyn D., Hetmanczyk M.P.: Estimation of pulsation of the sliding-vane pump for selected settings of hydrostatic system, Eksploatacja i Niezawodność – Maintenance and Reliability, vol. 17 nr 3, 2015, pp. 338-344.
3. Klarecki K., Rabsztyn D., Hetmanczyk M.P.: Influence of setting the selected parameters of hydraulic systems on pressure pulsation of gear pumps, Diagnostyka, Vol. 16, No. 2, 2015, pp. 49-54.
4. Kudźma Z. Damping of pressure pulsations and noise level in hydraulic systems in transient and established conditions. Wroclaw University of Technology Publishing, Wroclaw, 2012 (in Polish).
5. Mednis W., Wiśniewski P., Olszewski M.: Displacement and Throttle Control of Electrohydraulic Servodrive. Workshop to 4th International Fluidtechnisches Kolloquium "Intelligent Solutions by Fluid Power", Dresden 2004, s. 83–90.
6. Osiecki A.: Hydrostatic drive of machines. WNT. Warsaw 2014 (in Polish).
7. Stefański T., Zawarczyński Ł.: Energy-saving hydraulic drive with voltage inverter-fed induction motor. Acta Mechanica et Automatica, vol 4, nr 2/2010, pp. 130-136.

SELECTED ENGINEERING PROBLEMS
NUMBER 7
INSTITUTE OF ENGINEERING PROCESSES AUTOMATION
AND INTEGRATED MANUFACTURING SYSTEMS

Marek PŁACZEK

Institute of Engineering Processes Automation and Integrated Manufacturing Systems,
Faculty of Mechanical Engineering, Silesian University of Technology, Gliwice, Poland
marek.placzek@polsl.pl

EXACT AND APPROXIMATE METHODS IN ANALYSIS OF ONE-DIMENSIONAL MECHANICAL SYSTEMS

Abstract: Paper presents comparison of an exact Fourier method and an approximate Galerkin method in analysis of one-dimensional vibrating mechanical systems. Assumptions of the approximate method are presented. The considered systems are beams with different methods of fixing – different boundary conditions. Values of natural frequencies and dynamic flexibilities of considered systems are designated using the approximate method and compared with results obtained using the exact method.

1. Introduction

Considered one-dimensional systems are mechanical subsystems of the mechatronic systems with piezoelectric transducers used as vibration dampers or actuators [2,3]. Mechatronic systems were analyzed in other publications [1,2]. It is impossible to use the exact method to analyze mechatronic systems therefore the approximate method was used. Assumptions and verification of the approximate method was presented in [1]. The analyzed system was a cantilever beam with piezoelectric passive vibration damper. Presented method of system's fixing – one end clamped and one free, was chosen deliberately from all the possible ways of fixing because in this case inaccuracy of the approximate method is the highest among all the possible ways of fixing. The approximate method should be verify and corrected if necessary, so it is important to indicate what determines the uncertainty of the method and how to correct it. In this paper results obtained for two extreme cases are presented. In the first case (a simply supported beam) there is no differences between results obtained using the exact and the approximate method (values of natural frequencies are exactly the same), while in the second case inaccuracies of the approximate method are significant.

2. Analysis of considered mechanical systems

Considered mechanical systems are presented in Fig. 1 and Fig. 2. The first system is a simply supported beam and the second one is a cantilever beam. Both systems are loaded by the external harmonic force that operates perpendicular to the beam's axis. Boundary conditions of considered systems are presented in Tab.1.

Tab.1. boundary conditions of considered mechanical systems

Simply supported beam	Cantilever beam
$y(0,t)=0$, $\frac{\partial^2 y(0,t)}{\partial x^2}=0$, $y(l,t)=0$, $\frac{\partial^2 y(l,t)}{\partial x^2}=0$,	$y(0,t)=0$, $\frac{\partial y(0,t)}{\partial x}=0$, $\frac{\partial^2 y(l,t)}{\partial x^2}=0$, $\frac{\partial^3 y(l,t)}{\partial x^3}=0$,

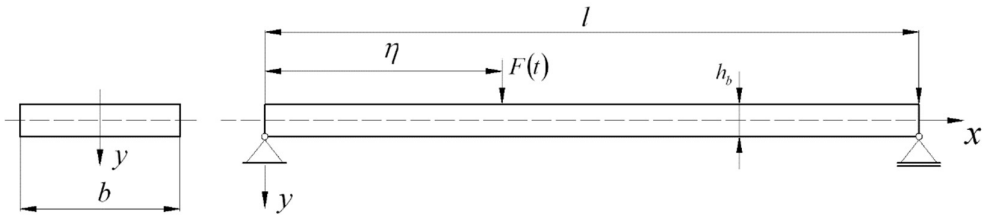

Fig.1. The first considered mechanical system - simply supported beam

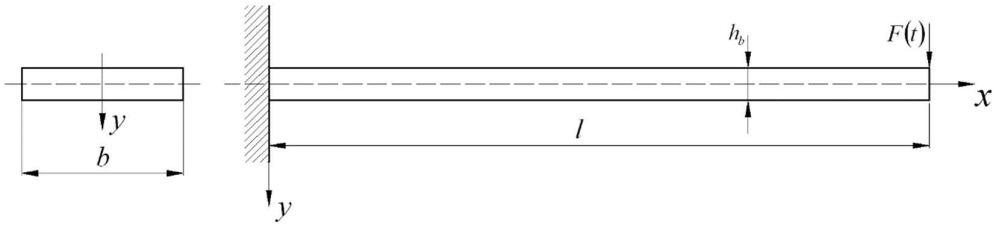

Fig.2. The second considered mechanical system - cantilever beam

In both cases equation of the beam's motion can be described as:

$$\frac{\partial^2 y(x,t)}{\partial t^2}=-\frac{EJ}{\rho b h_b}\frac{\partial^4 y(x,t)}{\partial x^4}+\frac{F(t)\delta(x-\eta)}{\rho b h_b}, \tag{1}$$

where: *E, J, ρ* are Young's modulus, moment of inertia and density of the beam. Dirac delta function $\delta(x-\eta)$ was introduced to describe the distribution of the externally applied force. Taking into account boundary conditions and equation of the beam's motion solutions of characteristic equations of both system were designated in agreement with the exact Fourier's method of separation of variables:

$\sin k_n l \cdot \sinh k_n l = 0,$ - for the simply supported beam and (2)

$$\cos k_n l = -\frac{1}{\cosh k_n l}, \qquad \text{- for the cantilever beam.} \tag{3}$$

Graphical solutions of these equations are presented in Fig. 3.

a)

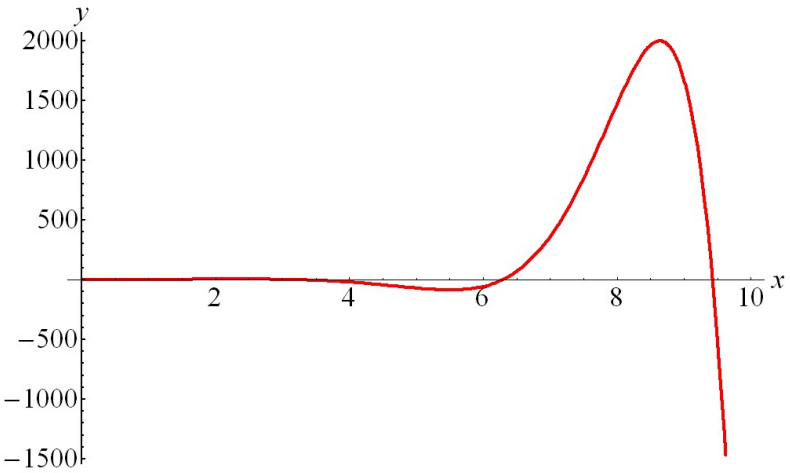

b)

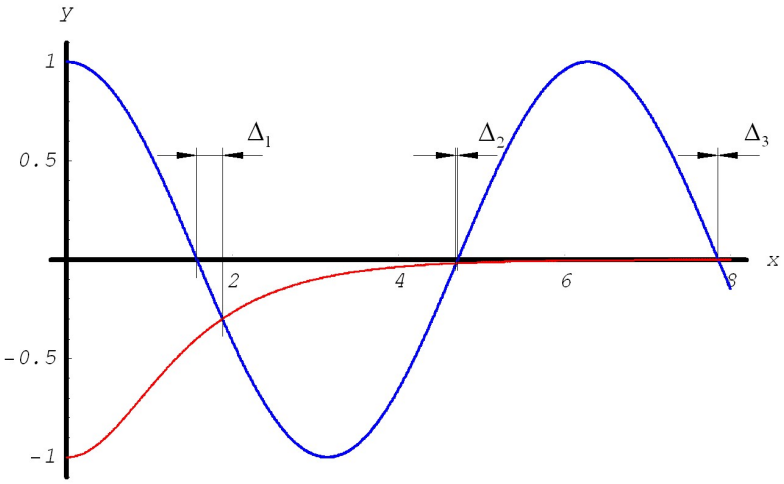

Fig.3. Graphic solutions of the characteristic equation, a) simply supported beam, b) cantilever beam

Taking into account graphical solutions of equations of motion of considered mechanical systems the equation of beams deflection in the approximate method for both systems was assumed as:

$$y(x,t) = \sum_{n=1}^{\infty} A \cdot \sin k_n x \cdot \cos \omega t, \tag{4}$$

where:

$$k_n = \frac{n\pi}{l}, \qquad n = 1,2,3... \qquad \text{- for the simply supported beam and} \qquad (5)$$

$$k_n = (2n-1)\frac{\pi}{2l}, \qquad n = 1,2,3... \qquad \text{- for the cantilever beam} \qquad (6)$$

A is an amplitude of the beam's vibration.

Equations of natural frequencies of considered systems obtained using the exact and approximate methods are presented in table 2. In this table inaccuracies of the approximate method are presented in percentage.

Tab.2. Obtained equations of natural frequencies of considered systems

Simply supported beam		Cantilever beam		
The exact and the approximate method	Δ[%]	The exact method	The approximate method	Δ[%]
$\omega_1 = \sqrt{\frac{EJ}{\rho A}}\left(\frac{\pi}{l}\right)^2$	0	$\omega_1 = \sqrt{\frac{EJ}{\rho A}}\left(\frac{1,8751}{l}\right)^2$	$\omega_1 = \sqrt{\frac{EJ}{\rho A}}\left(\frac{\pi}{2l}\right)^2$	29,8
$\omega_2 = \sqrt{\frac{EJ}{\rho A}}\left(\frac{2\pi}{l}\right)^2$	0	$\omega_2 = \sqrt{\frac{EJ}{\rho A}}\left(\frac{4,6941}{l}\right)^2$	$\omega_2 = \sqrt{\frac{EJ}{\rho A}}\left(\frac{3\pi}{2l}\right)^2$	-0,782
$\omega_3 = \sqrt{\frac{EJ}{\rho A}}\left(\frac{3\pi}{l}\right)^2$	0	$\omega_3 = \sqrt{\frac{EJ}{\rho A}}\left(\frac{7,85477}{l}\right)^2$	$\omega_3 = \sqrt{\frac{EJ}{\rho A}}\left(\frac{5\pi}{2l}\right)^2$	0,023
$\omega_{n>3} = \sqrt{\frac{EJ}{\rho A}}\left(\frac{n}{l}\pi\right)^2$	0	$\omega_{n>3} = \sqrt{\frac{EJ}{\rho A}}\left(\frac{2n-1}{2l}\pi\right)^2$	$\omega_{n>3} = \sqrt{\frac{EJ}{\rho A}}\left(\frac{2n-1}{2l}\pi\right)^2$	0

In the exact method equation of the beam's natural frequency was designated as the solution of the characteristic equation of the system. In the approximate method these equations were determined taking into account assumed equations (2) and (3). For the simply supported beam obtained equations are exactly the same, while for the cantilever beam there are inaccuracies for the first three natural frequencies.

Dynamic flexibility of considered mechanical system was designated using the exact and corrected approximate method. The dynamic flexibility α_Y is defined by equation [1,2]:

$$y(x,t)=\alpha_Y \cdot F(t). \tag{7}$$

Geometrical and material parameters of considered systems are presented in Tab. 3. Absolute value of obtained dynamic flexibility Y for the first three natural frequencies are presented in Fig. 4 for the simply supported beam and in Fig. 5 for the cantilever beam.

Tab.3. Parameters of considered mechanical systems

Geometrical parameters	Material parameters
$l=0{,}24[m]$, $b=0{,}04[m]$, $h_b=0{,}002[m]$, $\eta=0{,}01[m]$,	$E=210000[MPa]$, $\rho=7850\left[\frac{kg}{m^3}\right]$.

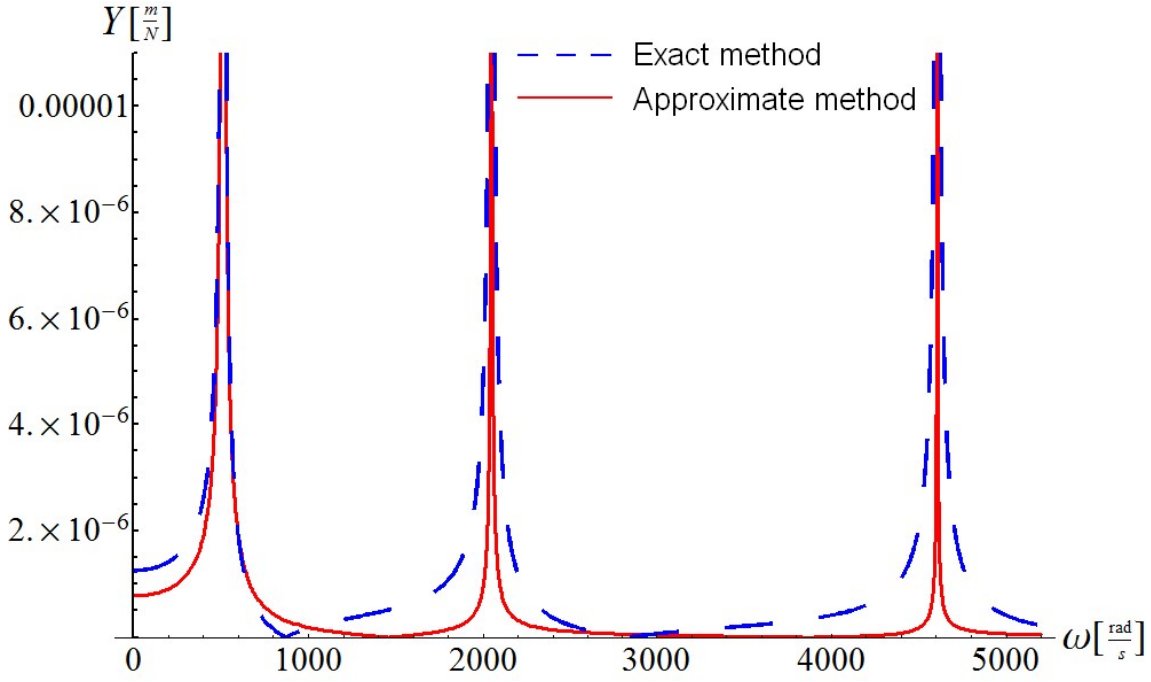

Fig.4. The dynamic flexibility of the simply supported beam, for n=1,2,3

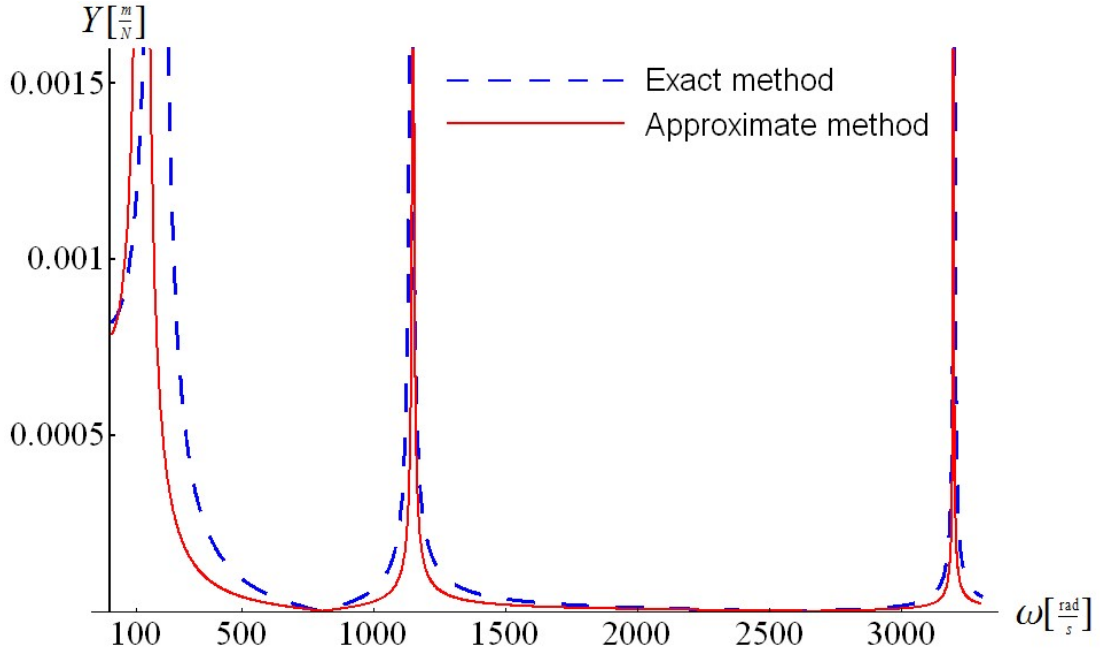

Fig.5. The dynamic flexibility of the cantilever beam, for n=1,2,3

3. Conclusions

It was proved that inexactness of the Galerkin method depends on the boundary conditions of the analysed system and assumed equation of the beam's deflection (equation 4). Considered systems were chosen purposely to show that in the first system the approximate method does not require correction while in the second one inaccuracy has to be corrected.

References

1. Buchacz A., Płaczek M.: The analysis of vibrating systems based on the exact end approximate method, International Journal of Modern Manufacturing Technologies, Vol. II, No 1, (2010), pp. 19-24
2. Buchacz A., Płaczek M.: Development of Mathematical Model of a Mechatronic System, Solid State Phenomena Vol. 164 (2010), Trans Tech Publications, Switzerland, pp. 319-322.
3. Maxwell N. D., Asokanthan S. F.: Modal characteristics of a flexible beam with multiple distributed actuators. Journal of Sound and Vibration 269 (2004), pp. 19-31.

SELECTED ENGINEERING PROBLEMS
NUMBER 7
INSTITUTE OF ENGINEERING PROCESSES AUTOMATION
AND INTEGRATED MANUFACTURING SYSTEMS

Dominik RABSZTYN

Institute of Engineering Processes Automation and Integrated Manufacturing Systems,
Faculty of Mechanical Engineering, Gliwice, Poland
dominik.rabsztyn@polsl.pl

EXPERIMENTAL TESTS OF THE INFLUENCE OF AIR ON THE PRESSURE PULSATION ON GEAR PUMP PRESSURE LINE

Abstract: The article presents results of preliminary experimental tests regarding the influence of phenomena resulting from the occurrence of air lock in the suction line on the pressure pulsation of a gear pump with external gear design, series PGP511 produced by Parker Hannifin. A cycle of measurements was carried out for four pressure values and fixed temperature of hydraulic fluid. The obtained test results were analyzed in domains of time and frequency.

1. Introduction

Despite considerable development in the area of drive technologies, users of the systems with hydrostatic drives still suffer from many failures resulting from air lock in the working medium. Air presence in the system is not only a significant threat for the correct functioning of the hydraulic system components such as pumps, valves and receivers, but also leads to physical and chemical changes in the working medium (increased compressibility, accelerated oxidation, deterioration of lubricating properties, acceleration of chemical decomposition of additives) [6, 8]. Air lock in the fluid results in reducing hydraulic rigidity of the drive and in turn leads to lowering the accuracy of positioning the receivers, especially in the systems with hydraulic servo valves and proportional valves [2, 3]. Air presence also leads to the generation of increased levels of noise and vibration of the drive unit [1, 4, 5, 7]. All this contributed to the necessity of analyzing the phenomena connected with the occurrence of air in the hydraulic systems.

This article focuses on the tests regarding the impact of leakage in the suction line, causing air lock in the working fluid on pressure pulsation in the pressure line.

2. Measuring station and experiment plan

A measuring system (Fig. 1) has been composed of a gear pump with external gear design (series PGP511 produced by Parker Hannifin) with the capacity of 8cm^3, powered by asynchronous AC motor with nominal rotational speed of 1500rpm, a throttle valve 9N600S (regulation of the hydraulic resistance). A leakage was introduced to the suction line

by means of the diagnostic conductor with inner diameter ϕ2mm and the length 1500mm. A pressure sensor HDA 4748-H-0250 was mounted at the pressure flange of the pump. Working fluid temperature (mineral oil HLP46) during the experiment was 40°C. Results of the experiment were saved using HYDAC HMG3010 measuring and data-acquisition device.

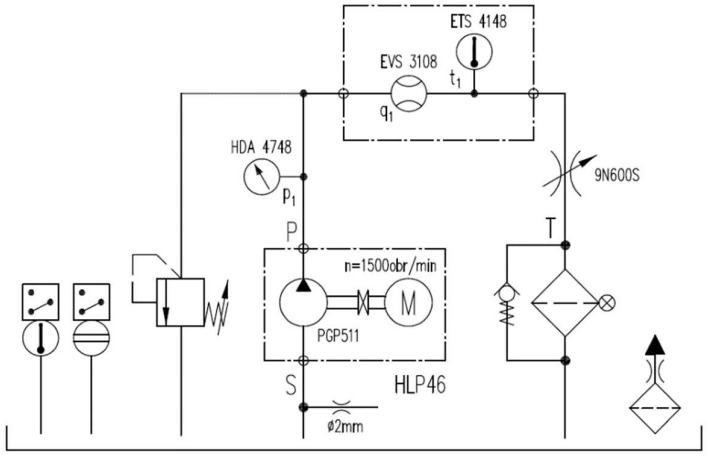

Fig. 1. Simplified hydraulic diagram of the measuring station

Measurements were carried out according to table 1. Variable parameters was pressure in the pressure line. A comparison of pressure pulsation has been made for the fluid with and without air pockets.

Table 1. Experiment plan

No	Designation of research	Pressure value [MPa]	Air lock
1	PC_50	5	No
2	PC_100	10	
3	PC_150	15	
4	PC_200	20	
5	ZC_50	5	Yes
6	ZC_100	10	
7	ZC_150	15	
8	ZC_200	20	

Analysis of air pockets in the suction line has been prepared in domain of time and frequency. The time analysis was carried out in order to determine the peak-to-peak value of pumping pressure that influences fatigue wear of the hydraulic system components and is responsible for generating increased levels of vibration and noise. The frequency analysis was carried out in

order to identify the irregularities of frequency response of the examined gear pump, which may be used to detect air pockets in the working fluid [3].

3. Results of experimental tests

Gearwheels of the PGP511 displacement pumps are fitted with 12 teeth; hence the frequency of the teeth engagement, equal to the frequency of the expected capacity fluctuation f_p, is 300Hz. The frequency f_p is connected with the frequency of pump shaft rotation f_n.
Table 2 presents the results for the pressure peak amplitudes, resulting from the pump shaft rotation f_n and the blades entering the pumping phase f_p. Frequency of sampling signals registered during the experiments was 10kHz. 16384 samples analyzed in the rectangular window were taken for the FFT-based data processing.

Table 2. Selected results of the experiment

No	Designation of research	Time domain analysis			Frequency domain analysis			
		p_{t_min} [MPa]	p_{t_max} [MPa]	Δp_t [MPa]	p_n for 25Hz [MPa]	p_p for 300Hz [MPa]	p_{f_max} [MPa]	Frequency f_{max} for p_{f_max} [Hz]
1	PC_50	4,95	5,04	0,09	0,006	0,032	0,032	300
2	PC_100	9,93	10,05	0,12	0,01	0,037	0,037	300
3	PC_150	14,97	15,09	0,12	0,013	0,038	0,038	300
4	PC_200	19,97	20,12	0,15	0,014	0,037	0,037	300
5	ZC_50	4,38	5,41	1,03	0,026	0,032	0,083	6
6	ZC_100	9,71	10,48	0,77	0,049	0,032	0,108	2,4
7	ZC_150	14,34	15,65	1,31	0,021	0,029	0,231	2,4
8	ZC_200	19,21	20,85	1,64	0,055	0,028	0,174	3,6

Selected pressure pulsation curves as a domain of time are presented in fig. 2 and 3.

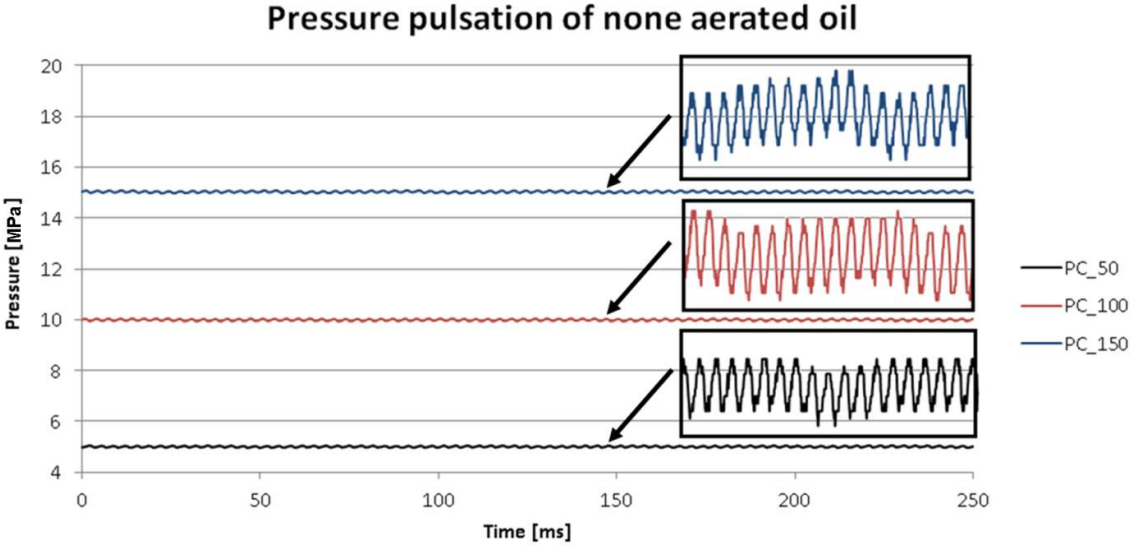

Fig. 2. Curves of pressure pulsation for the none aerated oil

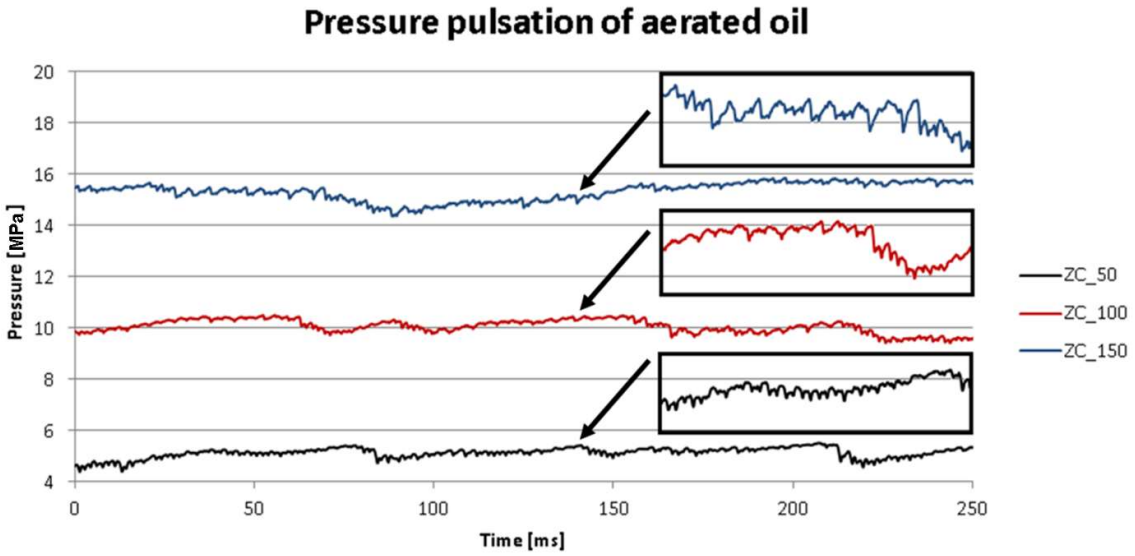

Fig. 3. Curves of pressure pulsation for the aerated oil

It should be remembered, that on the results of conducted experimental test affects not only the parameters of the pump, but also parameters of the pressure line, including bulk modulus of hydraulic fluid [5].

Frequency spectrums of pressure for experiments are presented in fig. 4 and 5.

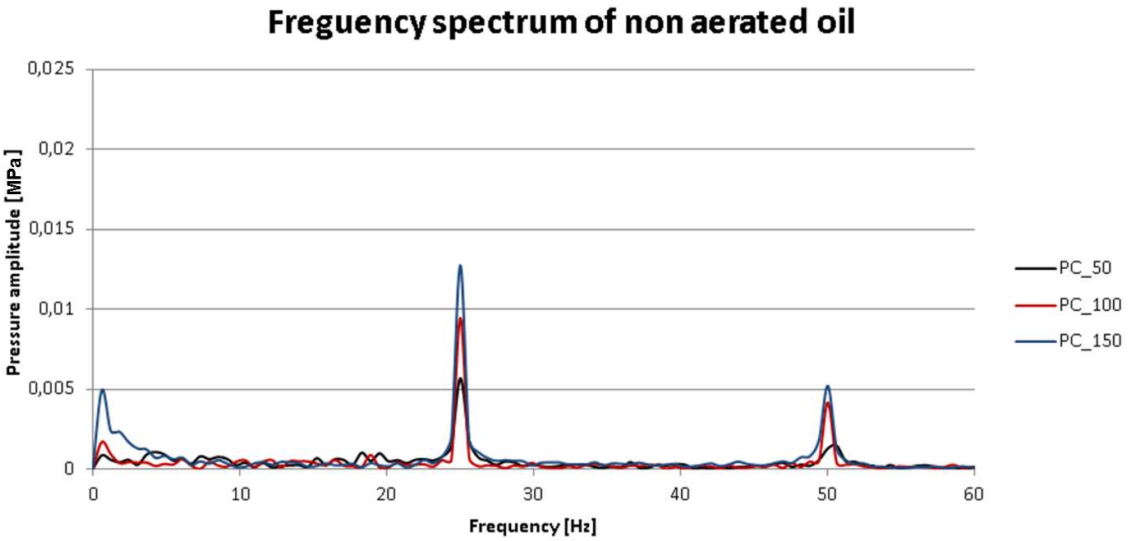

Fig. 4. Frequency spectrum for the none aerated oil

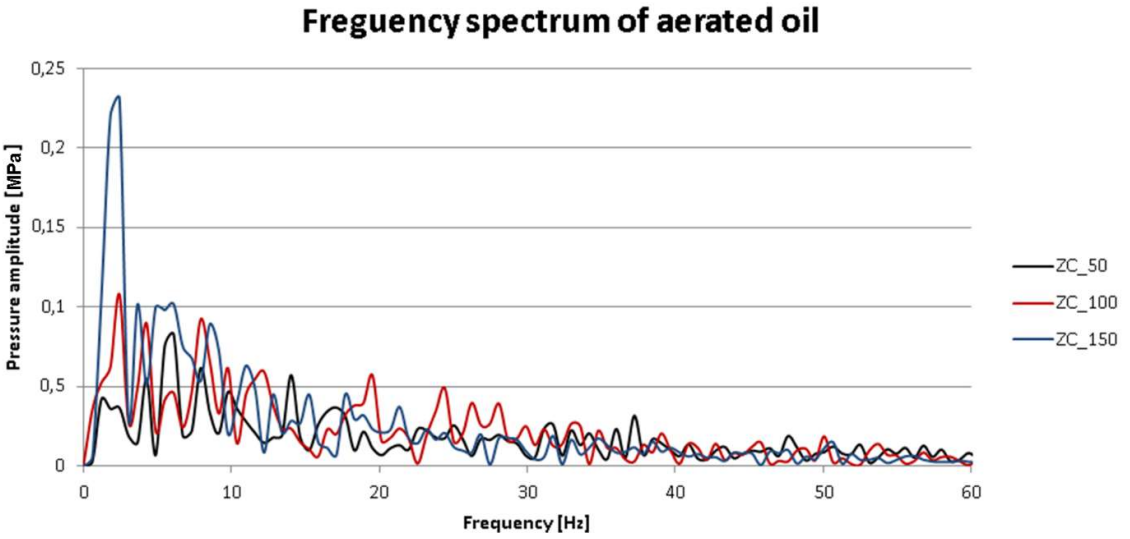

Fig. 5. Frequency spectrum for the aerated oil

4. Conclusion

Analyzing the curves of pressure pulsation as a domain of time, a significant increase (by an order of magnitude) of pressure peak-to-peak values was registered. Considerable differences in the curves of fluid pressure pulsation were observed. Fluid without air lock is characterized by the regularity of pressure curves, on the contrary to the fluid with air in it.

In case of the fluid without air lock, the amplitude of pressure pulsation resulting from temporary change of pump capacity caused by the teeth engagement is much higher than pulsation resulting from the pump gearwheel eccentricity. Increase of pressure values results in the increase of pressure pulsation amplitude resulting from the rotational speed of the shaft. The highest amplitude of pressure pulsation occurs for the frequency resulting from the teeth engagement (frequency 300Hz). In the fluid without air lock, in the range of low frequencies (below 20Hz), pressure pulsation was not observed.

Air lock in the suction line result in the significant increase in pressure pulsation on the pressure line. The highest amplitudes of pressure pulsation for the analyzed pressure values on the pressure line were registered at low frequencies. The air lock affects the dynamic changes of hydraulic fluid bulk modulus and leads to variation in pump pressure pulsation.

Considerable increase of pressure pulsation values resulting from air lock in the working fluid lead to the accelerated fatigue wear of the hydraulic system components.
The observed phenomenon requires additional tests.

References

1. Ickiewicz J. Hydraulic and mechanical vibrations of gear pump. Hydraulic and Pneumatics, 3/2013, pp. 12-16 (in Polish).
2. Klarecki K., Rabsztyn D., Hetmanczyk M.P.: Estimation of pulsation of the sliding-vane pump for selected settings of hydrostatic system, Eksploatacja i Niezawodność – Maintenance and Reliability, vol. 17 nr 3, 2015, pp. 338-344.
3. Klarecki K., Rabsztyn D., Hetmanczyk M.P.: Influence of setting the selected parameters of hydraulic systems on pressure pulsation of gear pumps, Diagnostyka, Vol. 16, No. 2, 2015, pp. 49-54.
4. Kollek W. , Kudźma Z.: Experience in the silencing machinery with the hydrostatic drive systems. Drives and Control, 6/2012, pp. 76-85 (in Polish).
5. Kudźma Z. Damping of pressure pulsations and noise level in hydraulic systems in transient and established conditions. Wroclaw University of Technology Publishing, Wroclaw, 2012 (in Polish).
6. Osiecki A.: Hydrostatic drive of machines. WNT. Warsaw 2014 (in Polish).
7. Stosiak M.: The influence of mechanical vibrations of the substrate on the pressure pulsation in the hydraulic system. Hydraulics and Pneumatics 3/2006, pp. 5-8 (in Polish).
8. Stryczek S.: Hydrostatic drive Vol. 1. WNT, Warsaw 1995 (in Polish).

SELECTED ENGINEERING PROBLEMS
NUMBER7
INSTITUTE OF ENGINEERING PROCESSES AUTOMATION
AND INTEGRATED MANUFACTURING SYSTEMS

Tetiana ROIK[1*], Iuliia VITSUK[2]

[1]Technology of Printing Production Department, Publishing Printing Institute, National Technical University of Ukraine "Igor Sikorsky Kyiv Polytechnic Institute", Kiev, Ukraine,
[2]Reprography Department, Publishing Printing Institute, National Technical University of Ukraine " Igor Sikorsky Kyiv Polytechnic Institute", Kiev, Ukraine,
[*]roik2011@gmail.com

THE EFFECTIVENESS OF MANUFACTURING TECHNOLOGY OF ANTIFRICTION COMPOSITE PARTS BASED ON NICKEL

Abstract: In a paper the research results of structural periodicity in the antifriction composite parts based on nickel with solid lubricant CaF_2 have been presented. The periodicity of structure was studied using Fourier analysis. Analysis of the structural status complexity and rheological characteristics of the friction surface was carried out by two-dimensional diffraction spectrum. This analysis determines the average size of structural components, the distance between them, the concentration and length of interphase boundaries. Fourier analysis method was used to check, prove and confirm the correctness of new composite antifriction parts' manufacturing technology. This method has shown the homogeneity of the composite material as a whole that proves the efficiency of the developed manufacturing technology. The developed technology provided the high tribological characteristics of the new parts for printing machines.

1. Introduction

Requirements for new wear-resistant parts are constantly increasing. This applies to both cast and powder parts. The main task in the development of new composite antifriction parts is to increase the life of machines and mechanisms, for example, printing equipment.

The known cast alloys based on copper, nickel (or cobalt) demonstrate unsatisfactory tribotechnical properties - high friction coefficient and wear at heavy-duty conditions of printing machines [1–5]. For example, it is known cast antifriction bronze bushings are able to operate only 0.5-1.0 year in printing machine' friction unit. After that catastrophic wear of bushing occurs.

Powder composite materials based on iron or alloy powder steel are known to be used at speeds $V<400$ rpm and loads up to 3.0 MPa. At higher speeds ($V\geq600$ rpm) and loads up to 1.5-5.0 MPa, materials based on nickel, cobalt and copper are used [1–7]. This is due to their original physical properties [2].

Materials based on nickel are well known among antifriction composite materials intended for severe operating conditions of higher loads and rotation speeds [1–5]. Studies have shown very good results and opened up prospects of the new antifriction bushings' industrial use in

the friction units of printing machines [2–5]. The developed manufacturing technology ensures a high level of properties for new composite antifriction parts based on powder nickel alloy EP975 with powders of solid lubricant CaF_2 [3, 4–7].

However, structural changes and other physical phenomena remained unexplored, that does not allow uniquely estimating the efficiency of manufacturing technology.

Therefore, the objective of the present paper is studying of the new composite parts' structural periodicity, the structural changes in the researched material based on powder high–alloyed nickel alloy EP975 with the solid lubricant CaF_2 powders by use the Fourier analysis method. Such approach gives a possibility to check, prove and confirm the correctness of new composite antifriction parts' manufacturing technology.

2. Experimental results and discussion

Examination Techniques. The object of the study was the composite antifriction material based on powder high–alloyed nickel alloy EP975 with the solid lubricant CaF_2 powders. Structure was studied using raster microscopy. The periodicity of structure was studied using Fourier analysis.

Method of determining the orientational anisotropy is as follows. Tensions of structure ordering can always be described by functions of the shift, rotation and changes of the periodicity, namely by functions $f(x, y, z)$, $f(\alpha, \beta, \gamma)$ and $P(x, y, z)$ accordingly. These characteristics reveal the degree of structure organization. They appear in the spectrum and can be registered and properly evaluated by scanning electron narrow beam on the investigated surface [8–10].

Fourier analysis of the resulting spectrum was performed using program SIA 1.00, adapted to the most modern computers. Two-dimensional Fourier spectrum is analyzed in this program.

Different areas of the structure reflect the scanning beam differently that causes change of the reflected signal.

The program works in two modes. In the first mode, the level of anisotropy and block's structure orientation quantitatively are estimated on the main operating tensions using autocorrelation and spectral analysis of surface fraktograms.

In the second mode the complexity of the structural state (the number of coefficients in the Fourier equation), the degree of anisotropy of main operating tensions and quantification of the degree of ordering structures on the friction surface (phase analysis) are qualitatively estimated in width and complexity of fraktograms. The angle between the axis of inertia and the abscissa for each image element is determined by direct scanning electron beam on the sample's surface.

In the reverse scan the histogram of chord length of image elements is calculated for each on the image angular ranges (0 to 180° at intervals of 10°).

Histogram is calculated by counting the hits number of the random value (in this case - the lengths of inertia axis on the image elements) into the specified classes.

Statistical analysis of the image elements orientation is summarized by the main orientation vector of image elements on the selected scan direction, coupled with the abscissa [9, 10].

Analysis of the structural status complexity and rheological characteristics of the friction surface was carried out by two-dimensional diffraction spectrum. This analysis determines the average size of structural components, the distance between them, the concentration and length

of interphase boundaries. It also allows exploring the anisotropy of the structure as a whole, which is associated with anisotropy of optical, mechanical and other properties.

The results of the comparative analysis from the surface histograms allow estimating the nature and size of the packaging structural elements, to carry out a comparative estimation of the studied surface anisotropy over the histogram width and the number of maximums at the same magnification and direction of scanning on the electron raster image.

We also carried out a qualitative analysis of the material texture for background characteristics such as brightness, size, shape, spatial orientation. The texture can be described by several features: fine grain, coarse, smooth, granulated, chaotic, linear, and so on. Texture is formed by external power factors and micrometallurgical processes. Textures characterize the stresses' orientation on the boundaries of structural components.

Thus, the objects of the study were new wear−resistant parts [2−4] based on powder high-alloyed nickel alloy EP975 with powders of solid lubricant CaF_2 (tab. 1.).

Tab. 1. Chemical composition of researched materials

Components, mass.%									
C	W	Cr	Mo	Ti	Al	Nb	Co	Ni	CaF_2
0.038–0.076	8.65–9.31	7.6–9.5	2.28–3.04	1.71–2.09	4.75–5.13	1.71–2.59	9.5–11.4	basis	4.0–8.0

Powders of the high-alloyed nickel alloy EP975 have been produced by powder spraying method of melted metal by argon stream. Dispersed metal drops are crystallized as spherical particles with dimensions from 10 to 750 μm [2].

The method of hot isostatic-pressing (HIP) was used for manufacture of new materials because the traditional technology of powder metallurgy doesn't ensure minimum porosity.

The process of hot isostatic pressing was carried out at 1210±10°C, during 4 hours, under pressure of argon up to 140 MPa.

Hot isostatic-pressing allows obtaining enough dense materials, almost without pores. The blanks had a relative density 99.9%.

After the hot isostatic pressing a heat treatment was carried out for optimization of dispersible phases' morphology in the structure of materials and for obtaining a necessary level of physical mechanical and antifriction properties.

Heat treatment includes hardening - heat to 1240°C during 4 hours, cooling with speed a 40 degrees/hour with a furnace to 1200°C, and then cooling on air.

After a hardening an ageing was carried out at 910°C during 16 hours on air.

HIP with a next heat treatment have been ensured the formation of phases in a structure, which increase material' physical-mechanical properties (combination of strength and plasticity) and improve operating reliability of antifriction part. Developed materials' tribotechnical, physical and mechanical properties have been presented in tab. 2 in a comparison with known powder Ni material, which is applied in analogue conditions [2].

Tab. 2. Mechanical and antifriction properties of new bearings based on alloys EP975

№	Composition, mass.%	Bending strength, σ_s, MPa	Impact resistance KC, J/m^2	Hardness, HB, MPa	Friction coefficient	Wear, μ/km (V=1200 rpm)
1	EP975+4% CaF_2	540−610	600−650	2550−2600	0,27	50
2	EP975+6% CaF_2	550−600	550−600	2500−2600	0,26	30
3	EP975+ 8% CaF_2	520−570	520−550	2540−2600	0,27	55
4	Ni+(18-45%) MoB_2+ ZrB_2)+ 5%(CaF_2 or BaF_2) sintered alloy [2]	240−300	350−520	850−950	0,31	180

Fourier analysis of the structure periodicity was caried out by scanning along the surface of the samples' thin sections using software packages for image analysis to confirm the effectiveness of the developed manufacturing technology. In studies we used two modes: the first - in secondary electrons, from surface's relief - mode SE (inelastic scattering) and the second - phase contrast - BE mode - in reflected electrons (elastic scattering).

Results of analysis at the direct and reverse scan are presented on fig. 1 and 2.

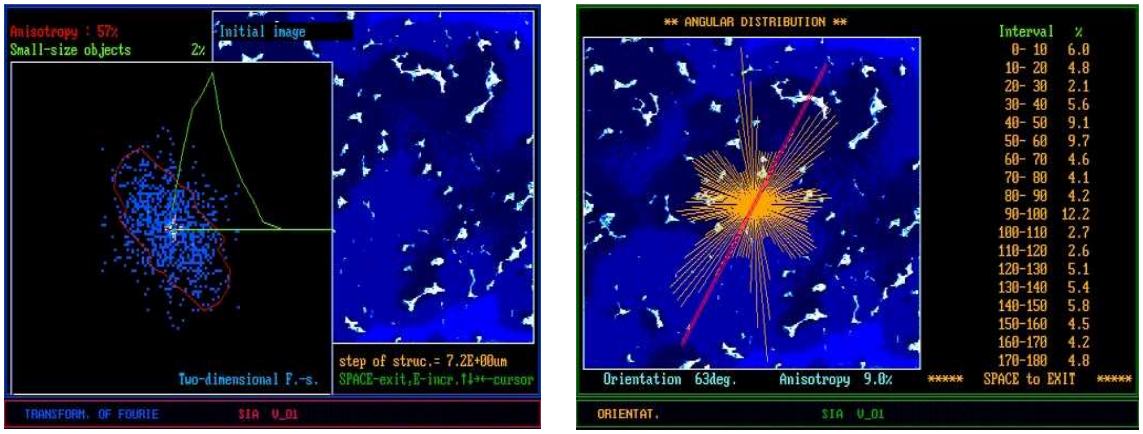

a *b*

Fig. 1. Fourier - analysis of the material EP975+8%CaF_2 structure (mode SE - the secondary electrons): a) structural (physical) anisotropy (direct scan); b) orientation of the alloy's particles (reverse scan)

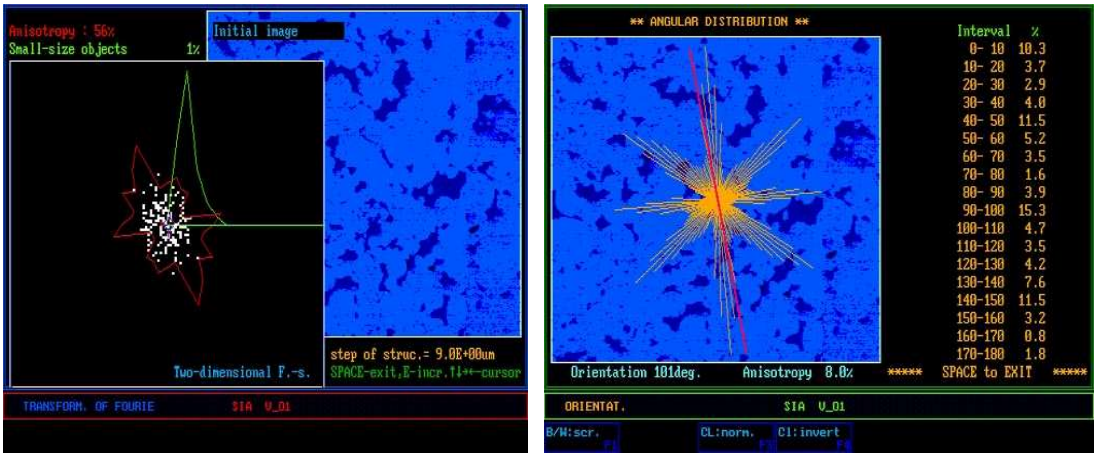

а *б*

Fig. 2. Fourier - analysis of the material EP975+8%CaF_2 structure in phase contrast (mode BE - the reflected electrons), depth from the surface to 50 nm: a) structural (physical) anisotropy (direct scan); b) orientation of the alloy's particles (reverse scan)

Tensions of structure ordering can always describe by functions of the shift, rotation and changes of the periodicity. These characteristics illustrate the degree of structure organization in material after manufacture. Also they are appeared in the reflected spectrum from the structural elements of composite material (from individual particles of researched material based on EP975+8%CaF_2), registered and quality evaluated at the scanning of narrow electron ray along analyzed surface of the sample. Since different parts of the structures are differed in their spatial orientation, they reflect differently scanning beam and it causes a change of the reflected signal.

Quantitatively it was estimated the structural (physical) level of anisotropy (fig. 1a, 2a) and orientation of the material's structural elements (geometric anisotropy) – Fig. 1b, 2b along the main operating tensions by analyzing the fraktograms of sample's surface, that is in the reflected electrons (depth ~ 50 nm) and in the secondary electrons – the surface relief. On fraktograms complexity we evaluated the structural status complexity (the number of coefficients in the Fourier equation), the degree of anisotropy (structural) of the main operating tensions, that is a result of hot pressing technology. We also obtained a quantitative estimation of the structural ordering degree in the material. Direct scanning method was used in both modes, SE and BE.

The angle between the inertia axis and the abscissa of each structural elements in the image was determined at the direct scanning of electron beam along the sample's surface (BE and SE modes), as shown in fig. 1a and fig. 2a.

At the reverse scanning (fig. 1b, 2b) we obtained the calculated histogram of the lengths of chords from structural elements in the image (particles of alloy EP975 and particles CaF_2) for each of the selected angular ranges in the image (from 0 to 180° at intervals of 10°).

A statistical analysis of the elements in images were obtained by the calculation in program SIA 1.00 of two-dimensional Fourier spectrum by counting the number of hits of a random variable at specified angular ranges (lengths of inertia axes of the structural elements in material). Then the obtained results were summarized by this program. So we got the main

orientation vector of structural elements on the selected scanning direction, coupled with the abscissa.

It was determined amount of the smallest structural elements (in %) and number of structural blocks for each angular range as a result of structural analysis and rheological features of the original material's surface (fig. 1b, 2b). This allowed us to estimate the anisotropy of the material structure in general.

The results of the structural elements distribution in the composite antifriction material based on powder Ni-alloy EP975 with solid lubricant CaF_2 have been presented in tab. 3.

Tab. 3. The distribution of the structural elements in the material EP975 + 6% CaF_2

Analysis mode	Fourier analysis		Orientation	
	$A_{str.}$, %	Small objects, %	Angle, degrees	$A_{aver.}$, %
SE surface relief (the secondary electrons)	57.0	2.0	63.0	9.0
BE - in reflected electrons, in phase contrast (depth 50 nm)	56.0	1.0	101.0	8.0

As research shows (fig. 1, 2 and tab. 3) the manufacturing technology ensured obtaining the dense deformed material (porosity ≈ 0.1%), as structural anisotropy evidenced (real physical anisotropy, $A_{str.}$), which is 57 and 56% according to analysis places – on the surface and in the volume of the sample (SE, BE modes).

The material shows almost the same level of physical anisotropy on the sample's surface after its mechanical grinding during preparation process, and in volume, since the depth of ~ 50 nm. This shows the homogeneity of the composite material as a whole.

Structural anisotropy is 57% directly from the surface of the sample, which is possibly due to its slight increase at the fine grinding of the sample. This is also evidenced by the increasing of angle inclination from 63^0 to 101^0 for the main orientation vector of the material's structural elements.

In this case, average geometric anisotropy (orientation, $A_{aver.}$) is very low – 9.0 and 8.0% regardless of the analysis mode (SE or BE). It illustrates the uniform arrangement of powder alloy's particles in all its volume and confirms the high voluminous homogeneity of the obtained material structure. Such structure is the result of technology HIP. The presence of small inhomogeneities (anisotropy) is confirmed by studies of physical mechanical and tribotechnical properties (tab. 2). Wear of the material takes play evenly across the surface friction.

The distribution of solid lubricant CaF_2 particles is characterized by uniformity in the material (Fig. 1, 2), which promotes the formation of stable secondary structures (friction films) on the contact surfaces. It can ensure a high level of the material's functional properties. This, in turn, minimizes wear and stabilizes a friction pair's operation.

The texture of examined materials was formed by external technological factors – temperature and loading parameters during the manufacturing process (except biographical

original signs when alloy EP975 was remelted and sprayed on the powder particles). That is, the fine grain structure was formed after manufacturing of the composite material by the developed technological process, as shown in fig. 1 and 2. Such structure ensures a high level of mechanical and tribotechnical properties (tab. 2) [2, 4].

Thus, the executed complex Fourier analysis of structural periodicity have confirmed the efficiency of the manufacturing technology of antifriction composite parts based on powder nickel alloy EP975. The developed technology can ensure a high and stable level of the antifriction parts' functional properties.

3. Conclusion

Thus, we had studied the structural changes and other physical phenomena in the antifriction composite parts based on powder nickel alloy EP975+CaF_2. In our research we used the Fourier analysis method. This method has shown almost the same level of physical orientational anisotropy on the sample's surface after its mechanical grinding during preparation process, and in volume, since the depth of ~ 50 nm. This shows the homogeneity of the composite material as a whole. The Fourier analysis method had confirmed the efficiency of new composite antifriction parts' manufacturing technology. The developed technology provided the high tribological characteristics of the new parts for printing machines.

References

1. A. P. Gavrish, P.O. Kyrychok, T. A. Roik, O. V. Zorenko, V. G. Oliynik "Precision grinding and polishing of the parts from high alloyed composites for printing machines: Monograph, [in Ukrainian], NTUU „KPI", Kyiv, 498 p. (2016).
2. T. Roik, A. Gavrish, P. Kyrychok, Iu. Vitsuk, M. Askerov "Physical Mechanical and Tribotechnical Properties of New Composite Bearings for Printing Equipment"//Journal of Science of the Gen. Tadeusz Kościuszko Military Academy of Land Forces, Wroclaw, Poland. -№2 (172), p. 141-149, (2014).
3. T. Roik, A. Gavrish, P. Kyrychok, Y. Vitsuk "Effect of making technology on the antifriction properties of new bearings for printing machines"//Selected engineering problems, Silesian University of Technology, Faculty of Mechanical Engineering, Gliwice, Poland, №4, p. 147-152, (2013).
4. T. A. Roik, A. P. Gavrish, P.O. Kyrychok, et al., Composite Bearing Material [in Ukrainian], Ukrainian Patent No. 60521, IPC (2009), C22C9/02, Bulletin No. 12, Publ. June 25 (2011).
5. T. A. Roik, A. P. Gavrish, P.O. Kyrychok, Iu. Vitsuk "Effect of secondary structures on the functional properties of high-speed sintered bearings for printing machines"//Powder Metallurgy and Metal Ceramics.- Springer/New York: Volume 54, Issue 1, p. 119-127, (2015).
6. T. Roik, A. Gavrish, Iu.Vitsiuk, O. Khlus "Friction behavior of the new composite bearing materials for printing machines and special use at heavy operating conditions"//Journal of Science of the Gen. Tadeusz Kościuszko Military Academy of Land Forces, Wroclaw, Poland. -Volume 47, Number 4 (178), 100-108, (2015).

7. T. Roik, A. Gavrish, Iu. Vitsuk “Effect of the friction films’ tribosynthesis mechanism on the antifriction properties of composite materials based on nickel”//Selected engineering problems, Silesian University of Technology, Faculty of Mechanical Engineering, Gliwice, Poland. - № 6, 81-90, (2015).
8. A. Enrique, V. Gonzalez "Connections in Mathematical Analysis: The Case of Fourier Series"// American Mathematical Monthly, Vol. **99** (5), p. 427–441, (1992).
9. L. N. Thibos, W. Wheeler, D. Horner “Power vectors: an application of Fourier analysis refractive error// Optometry and Vision Science, Vol. 74, № 6, p. 8, (1997).
10. P. L. Butzer, R. J. Nessel “Fourier analysis and approximation: Monograph, Academic Press Inc., New York− London, Vol. 1, 555 p., (2011).

SELECTED ENGINEERING PROBLEMS
NUMBER 7
INSTITUTE OF ENGINEERING PROCESSES AUTOMATION
AND INTEGRATED MANUFACTURING SYSTEMS

Mateusz SUMERA, Mariusz Piotr HETMAŃCZYK[1*]

[1]Institute of Engineering Processes Automation and Integrated Manufacturing Systems, Faculty of Mechanical Engineering, The Silesian University of Technology, Gliwice, Poland
[*]mariusz.hetmanczyk@polsl.pl

THE LABORATORY STAND FOR OPTIMIZATION OF SWING VALUES OF THE PHYSICAL PENDULUM – CONFIGURATION

Abstract: The article shows main features of the laboratory stand used for testing and optimization of swing values of the physical pendulum. Mechanical design, electrical protection arrangements and overall configuration were also described. The main goal was to develop the physical pendulum model driven by a synchronous servomotor (providing high rotational speed, efficiency and dynamic of operating parameters). Described model refers to industrial overhead cranes, especially in cases where unfavourable phenomenon of fluctuations of manipulated objects exists.

1. Introduction

Transportation and manipulation of physical objects suspended on flexible connectors require usage of specialized algorithms implemented in control systems (e.g. damping of angular displacement, reliable and fast readjustment of control parameters etc.). In the considered case a manipulated object can be treated as the physical pendulum (i.e. system in which the rigid body can perform a movement around the axis of rotation O, not passing through the centre of mass S, under the influence of gravitational forces). A resultant of gravitational forces which act on the elementary mass of the pendulum is proportional to the weight of the pendulum (Fig. 1). Oscillations of the physical pendulum belong to the periodic movement i.e. changes of the physical quantities recurring at regular time intervals [1,2].

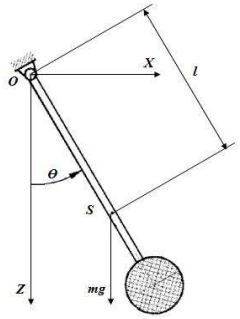

Fig.1. A schematic diagram of a physical pendulum [2]

The equations of motion of the physical pendulum pulled out from the equilibrium position by an Θ angle could be described by the following features [1,2,5,6]:

- a torque derived from the force of gravity:

$$M = -mglsin\Theta$$

- equation of motion:

$$I_0 \frac{d^2\theta}{dt^2} = -mglsin\theta$$

- simplification - reducing movement of the pendulum for small deflections (a few degrees) allows to expression angular values by means of the radian measure (i.e. sinθ≈θ):

$$\begin{cases} \frac{d^2\theta}{dt^2} + \frac{m \cdot g \cdot l}{I_0} = 0 \\ \omega_0 = \sqrt{\frac{m \cdot g \cdot l}{I_0}} \end{cases}$$

- oscillation period of the pendulum (in case of small angles of swings):

$$\begin{cases} T = \frac{2\pi}{\omega_0} \\ T = 2\pi \cdot \sqrt{\frac{I_0}{m \cdot g \cdot l}} \end{cases}$$

where:

M - moment of force $[Nm]$,
m - mass of a physical pendulum $[kg]$,
g - gravitational acceleration $[\frac{m}{s^2}]$,
l - distance between a centre of gravity and an axis of rotation $[m]$,
Θ - tilting angle [°],
I_0 - moment of inertia of a pendulum terms to the pivot axis $[kgm^2]$,
ω - angular frequency $[\frac{1}{s}]$,
T - oscillation period $[s]$.

Due to occurrence of additional forces acting on oscillator (e.g. air resistance, friction, dynamic forces caused by rapid change of speed and direction) a phenomenon of pendulum movement damping exists. In the real systems described features may have an impact on [3,4]:

- bevelling of gantry bridges - causing occurrence of additional stresses in structures (especially inside guides) and uneven weight distribution of crane construction (with special emphasis on supporting elements and guides),
- lack of precision in manipulation of loads to designated locations,

- complex process of manually elimination of adversely fluctuations, leading to machine damage and dangerous operational states.

2. The mechanical design of the laboratory stand

The frame and supporting elements have been made of aluminium extrudes sections with dimensions 45x45 millimetres (Fig. 2). The drive unit has been built through the use of a high precision rolled ball screw (the Bosch Rexroth BASA/40x10Rx6 model, Fig. 2) with the nominal diameter equals 40 millimetres and the 10 millimetres thread pitch.

The screw is characterized by high work precision as a result of small clearances existing between a single flange nut (FEM-E-C type, Fig. 2) and the ball screw (stabilized by using two bearing blocks).

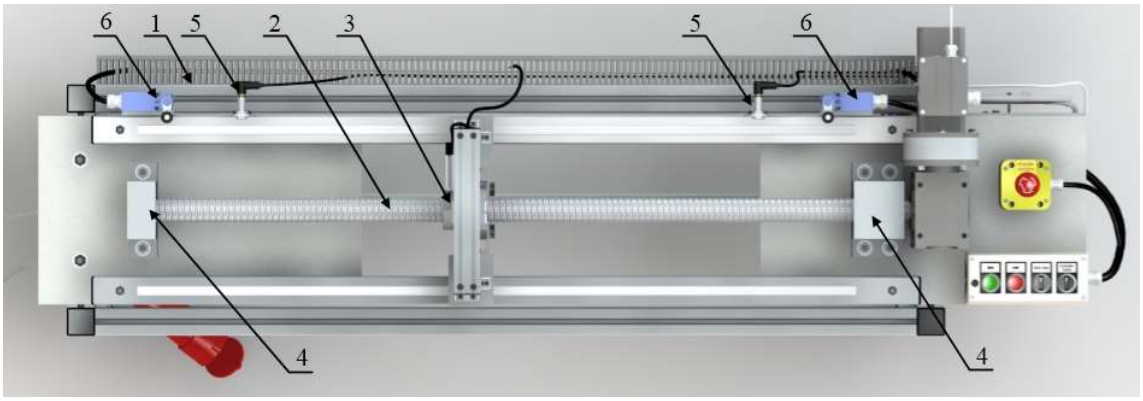

Fig.2. Top view of the 3D model, where: 1 - a cable tray, 2 - the high precision rolled ball screw, 3 - the nut, 4 - bearing blocks, 5 - inductive sensors, 6 - mechanical limit switches

A frame of the physical pendulum has been made of aluminium extrudes sections (cross-sectional dimensions equal 20x40 millimetres) and dedicated coupling brackets. The assembly has been placed on high precision guides (Fig. 2) allowing accurate and stable positioning realized on the motion plane.

The driven saddle is moved by a nut with mounting flange. Total length of guides equals 1139 millimetres, however, due to the spacing of the bearing blocks the total useful distance is limited up to 1100 millimetres.

The laboratory stand has undergone modernizations in order to satisfy stated assumptions. The first stage of the modernization concerned a durable fixation between the DFS56M servomotor and applied worm gear (made by the Chiaravalli, CHM-50 model). Such correction arises from size differences between diameters of mounting flanges and spacing of mounting holes (Fig. 3).

Frame of the physical pendulum was characterized by insufficient stiffness, this phenomenon was visible especially in cases of forced swings with simultaneous linear movements. Therefore, mounting brackets of the top sections were replaced by rigid screw fixings. To strengthen mechanical connections between vertical profiles and profiles of the driven saddle, additional stabilizing brackets were used (Fig. 4).

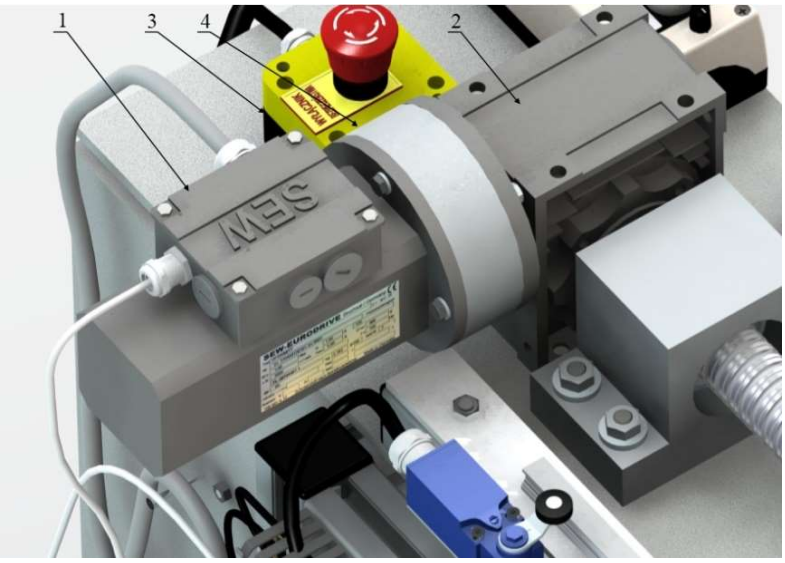

Fig. 3. View of complete drive system, where: 1 - electric servomotor, 2 - worm gear, 3 - safety switch, 4 - mounting adapter

Strengthening was made also between sections located on the sledges, which due to their construction are susceptible to deformation (on grounds of oscillations and rapid movements).

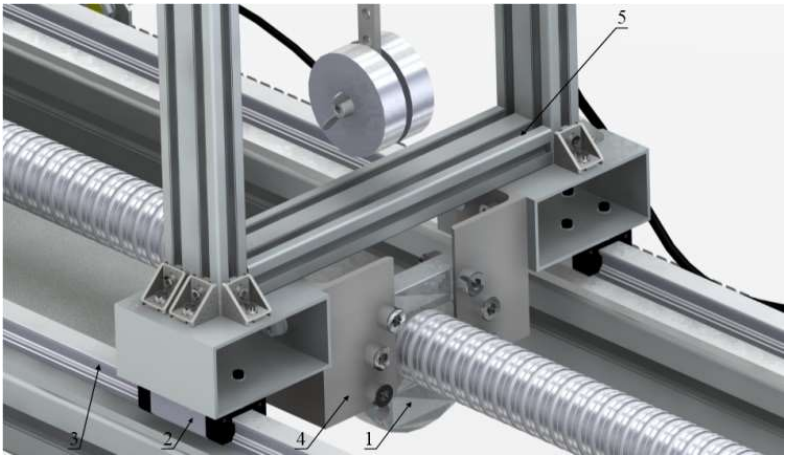

Fig.4. View of linear powertrain system, where: 1 - the single flange nut, 2 - a linear bearing, 3 - guides 4 - fasteners, 5 - a cross profile

The construction of the pendulum (Fig. 5) has been made of a flat steel bar with holes for changing the height position of test masses. Load are two aluminium discs with holes in axis, screwed on opposite sides of an arm.

Improvement of motion properties of the pendulum has been obtained by usage of rolling bearings in rotary joints (Fig. 5). This solution allows for an elimination of movement resistances, lateral looseness and vibrations. Rigidity of the structure and a lack of interferences caused by misalignment of the pendulum structure are essential aspects that guarantee the correctness of inclination measuring.

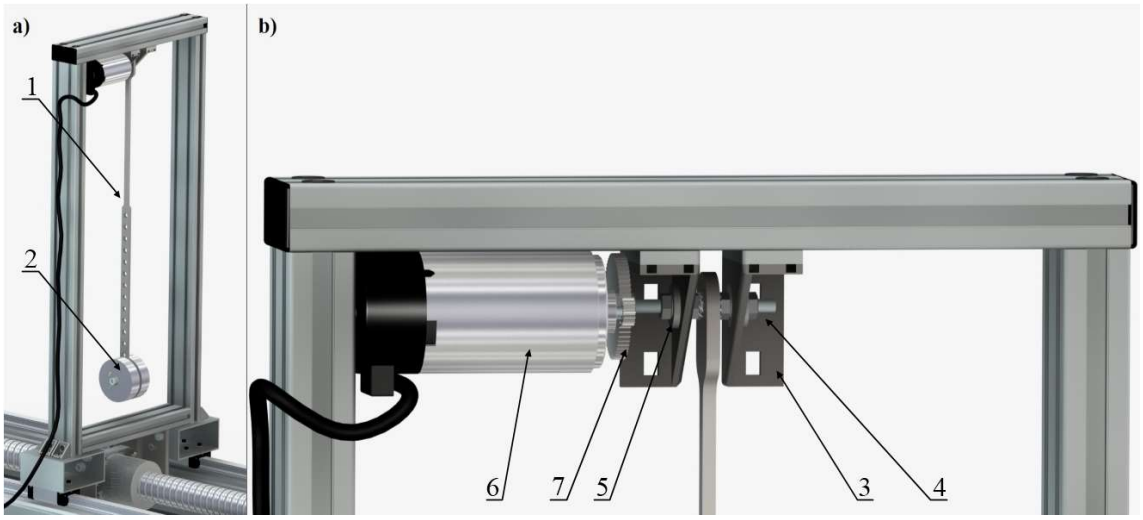

Fig. 5. View of the physical pendulum model: a) the frame, b) the clamping unit, where: 1 - the frame of the pendulum, 2 - test masses, 3 - mounting brackets, 4 - rotary axis, 5 - ball bearings, 6 - an encoder, 7 - a gear

In figure 5b an assembly of the sensor for measuring an inclination angle of the physical pendulum was shown.

3. Protection and electrical system

Described laboratory stand belongs to a teaching equipment what implicates a necessity of usage of additional safeguards against uncontrolled movement of a drive (especially at the top speed leading to a collision of the pendulum with one of the bearing blocks). For this purpose safety system has been equipped with two inductive sensors (TURCK model BI4-M12-AP6X-H1141, Fig. 6) with outputs configured as NO (Normally Open).

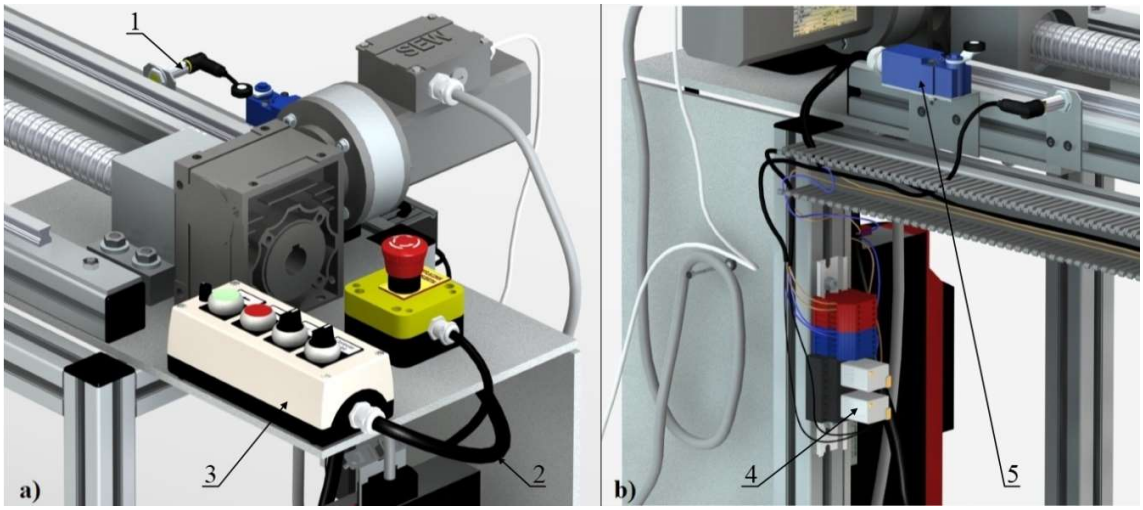

Fig. 6. View of the control system configuration: a) top view, b) view of the power module, where: 1 - inductive sensors, 2 - cable covers, 3 - a control box, 4 - relays, 5 - a limit switch

These sensors were programmed as non-contact bumpers, acting at the time of entry and detection of driven saddle (the control algorithm jumps immediately to emergency stop mode or change direction).

Such connection does not provide a secure execution of safety function in case of loss of communication with the PLC controller or other perturbation in control algorithm. Inductive sensors are connected directly to the binary inputs of the frequency inverter through relays. Due to the fact that they perform safety functions are required normally closed outputs. For this reason relays have been used.

This disadvantage was eliminated by a series connection of additional limit switches (Fig. 6) to the inputs X17 in the frequency converter, which serves as a safe disconnection of torque STO (Safe Torque Off).

4. Conclusions

In order to simulate a process of damping (in terms of different control algorithms realized by electric motors operated via frequency inverters) the model used to study a swing position of the physical pendulum was constructed. Described laboratory stand belongs to a teaching equipment but enables testing of advanced algorithms for damping of oscillations (elements hung on susceptible connectors).

The laboratory stand has been equipped with doubled safety functions (inductive sensors and XCKN2118P20 mechanical limit switches, produced by the Telemechanique), which are configured as NC (Normally Closed). Taken serial connection of two limit switches and safety button, prevents collisions.

References

1. Magiera A.: Physical laboratory. Krakow: Institute of Physics of Jagiellonian University, 2012.
2. Mianowski B.: Determination of the period of small and large swings of physical pendulum. Lodz: Publishing House of Technical University of Lodz, 2009.
3. Nowak A.: Modelling of dynamics driving bridge crane, taking into account the rebound phenomenon. Gliwice: The Silesian University of Technology Publishing House, 1995.
4. Kosucki A.: Research cargo transportation using associated movements of overhead cranes mechanisms. Lodz: Scientific Papers of the Technical University of Lodz, 2013.
5. Adams M.L.: Rotating Machinery Vibration: From Analysis to Troubleshooting (2nd Edition). New York: CRC Press, 2009.
6. Bently D.E., Hatch C.T.: Fundamentals of Rotating Machinery Diagnostics (Design and Manufacturing). USA: ASME Press, 2003.

SELECTED ENGINEERING PROBLEMS
NUMBER 7
INSTITUTE OF ENGINEERING PROCESSES AUTOMATION
AND INTEGRATED MANUFACTURING SYSTEMS

Mateusz SUMERA, Mariusz Piotr HETMAŃCZYK[1]

[1]Institute of Engineering Processes Automation and Integrated Manufacturing Systems, Faculty of Mechanical Engineering, The Silesian University of Technology, Gliwice, Poland
*mariusz.hetmanczyk@polsl.pl

THE LABORATORY STAND FOR OPTIMIZATION OF SWING VALUES OF THE PHYSICAL PENDULUM - CONTROL SYSTEM

Abstract: The article presents algorithms used to control swings of the physical pendulum. The division of control function blocks and a configuration of the control system were also described. The configuration contains a set of control algorithms, a PLC controller and a frequency converter. Additional element is a visualization of states, especially the drive system, allowing forcing and reading control signals. The configuration parameters of the equipment and industrial network were also shown.

1. Introduction

Development and optimization of control algorithms used in transportation equipment constitutes one of the main tasks in modern production systems [1,4]. Minimization of fluctuation impacts of transported elements results in improving the flow of process, reduction of energy consumption and increasing the safety of handling systems.

The laboratory stand has been designed to optimize swing values of physical pendulum. Physical model is equipped with components enabling realization of the control process with very high accuracy what has been achieved also through implementation of advanced algorithms. Communication between devices is made using PROFINET network, which provides the required data rate and reliability.

2. The control configuration and the drive subsystem

The control subsystem has been built with the following components (Fig. 1): the MDX61B0008-5A3-4-00 frequency inverter (with the DFE32B and the DER11B optional cards), the SIEMENS SIMATIC S7-1200 PLC controller (CPU 1214C DC/DC/DC, 6ES7 214-1AG31-0XB0), the HMI panel (Siemens KTP600 Basic Colour PN 6AV6 647-0AD11-3AX0).

The developed algorithms can be executed in different modes:

- the manual mode with a buttons control,
- the automatic mode (continuous run between end sensors),
- the PLC mode (control is done by the PLC controller connected with the KTP600 HMI panel)

Fig. 1. View of 3D model of the laboratory stand (a mechanical subsystem and control units)

In order to define the operating parameters of the electric motor, a configuration of the frequency converter was done. For this purpose, the MOVITOOLS MotionStudio was used. Parameterization was performed with usage of the Start-up environment but additional configurations were modified by using the Parameter Tree (Fig. 2).

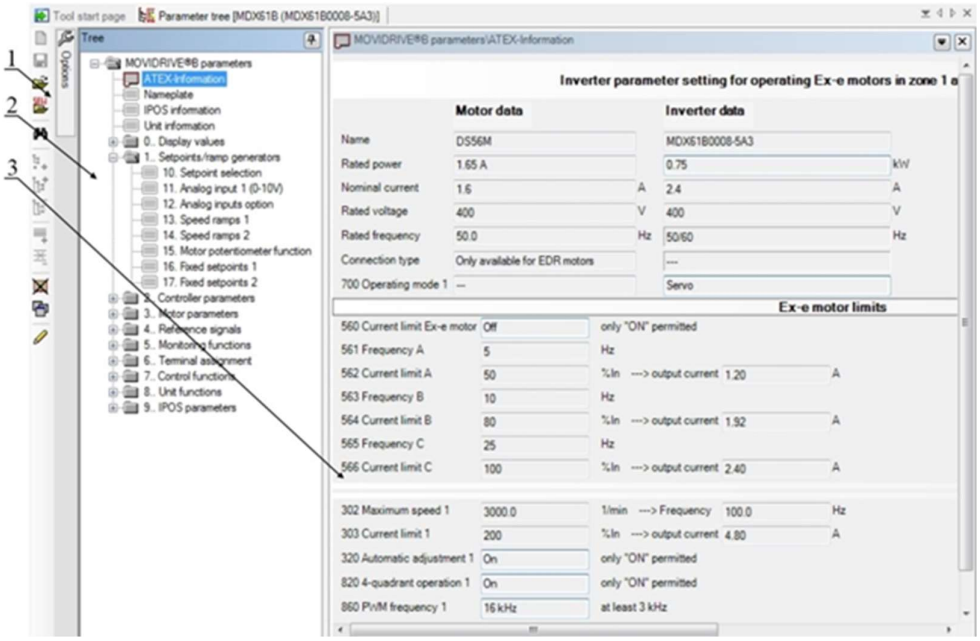

Fig. 2. View of main functions of the Parameter tree, where: 1 - ribbon options 2 – the parameter tree, 3 - a view area of selected parameters

All of the SEW inverters are equipped with an integrated positioning and sequence controller programmed by the IPOSplus language [5]. Prepared programme contains all the necessary commands required to perform a control process, communication via PROFINET,

appropriate cooperation with the PLC controller and exchange of operating parameters via MoviLink channel. An example of the program that provides control with usage of manual mode is shown in listing 1.

Code listing 1. An automatic mode code

```
Auto()
  { if (LS_R == 0)
    {
     _BitClear(ControlWord, 2);
     _BitSet(ControlWord, 3);
    }
    if (LS_L == 0)
    {
     _BitClear(ControlWord,3);
     _BitSet(ControlWord, 2);
    }
  }
```

movement in left direction

movement in right direction

The process of motion control is done by a corresponding change in the value of the control word (No. H484), which individual bits trigger relevant functions (e.g. a permit for movement, direction of rotation etc.).

The controller programming was carried out in the Siemens TIA PORTAL environment. The hardware configuration is shown in figure 3. New devices have been added by the function Devices&Networks from the project tree. Created system represents a physical connection of devices in the PROFINET network, identification of given device is realized by the IP address and a device name.

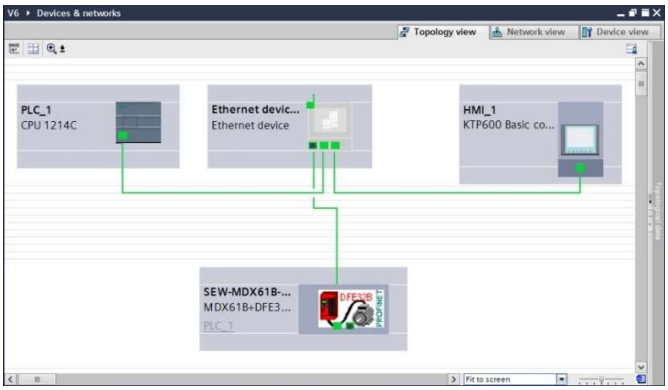

Fig. 3. View of the Configuration tree

Listing 2 shows a skeleton of the main block, by means of which are called several function blocks that enable implementation of the program. Described block is performed on the basis of conditional statements (IF) which check the actual condition (the status of the inverter - fault or warning). With the proper operation of the frequency inverter, described block is subjected to continuous processing (used to determine the parameters of the pendulum block and process variables associated with operational states of electric drive). Instruction of multiple-choice (CASE) is used for control mode selection. The condition scans variable "Ride_Type" refreshed by the master unit, based on preset settings.

Code listing 2. Structure of the Main (OB) block

```
(*Receiving of data packages*)
"Communication_Receive"(Hardware_ID:="DB_Control"….);
(*Control functions*)
IF NOT "DB_Control".Drive.PI.Fault_Warning THEN
    "DB_Control".Drive.PO.Controller_Inhibit := False;
 (*Pendulum Cycle*)
    "Period_FB_DB"(Number_Swings=>"DB_Control"….);
 (*Control mode*)
    CASE "DB_Control".HMI_Control.Ride_Type OF
       0: (*Main Screen*);
       1: (*Hand_Mode*);
       2: (*Automatic_Mode*);
       3: (*Pendulum*);
       4: (*Reference_Travel*);
    END_CASE;
 (*Dane*);
ELSE
    "DB_Control".Drive.PO.Stop := False;
    "DB_Control".Drive.PO.CW := False;
    "DB_Control".Drive.PO.Controller_Inhibit := True;
    "DB_Control".Drive.PO.WORD_EMPTY := 1;
END_IF;
(*Sending of data packages*)
    "Comunnication_Transmitter"(Hardware_ID:="DB_Control"….);
```

For the PLC controller and the HMI panel following control modes have been implemented:

- a manual mode - the driven saddle movement with parameter values defined by preset settings, movement to the determined position,
- the automatic mode - movement between end sensors or between programmed positions,
- the vibration optimization mode of the physical pendulum - movement on the basis of direct information from angle sensor or movements due to predicted consecutive values of swing angles.

Optimization of the pendulum swing is achieved by usage of one of the algorithms presented in code listing 3.

Code listing 3. Structure of the Pendulum_FB function block

```
CASE #HMI_Pendulum_Algorithm OF
1: Algorithm Encoder;
2: The dampening algorithm of harmonic distortion
  CASE #HMI_Pendulum_Ride OF
   1: Unilateral damping;
   2: Bilateral damping;
   END_CASE;;
END_CASE;
```

The main task of the algorithm is a compensation of the current tilt of the oscillator and application of the drive to damping of movements (based on feedback from the encoder).

The algorithm starts the initialization process, whose aim is to drive a saddle with pendulum to the centre position. Thereafter, method assumes movement between the end sensors at a constant speed of 1000 rpm in the automatic mode. In case of swing of the pendulum from its original position the control system performs a process of movement damping. Obtaining proper operation requires the speed damping.

The principle of work of the damping algorithm consists in determining the angle of swing of the physical pendulum, which will be reached at the next movement based on the characteristics of earlier inclinations.

For this purpose the equation of harmonic vibrations damping was implemented. The control algorithm allows prediction of value of vibration characteristics in time. Used algorithm allows to determine the Θ angle (between the arm and an axis of rotation of the oscillator).

Damping factor (Code listing 4) determines atrophy level of vibrations (with the growth of coefficient value the vibrations are damped in a shorter time). The vibration amplitudes are taken from the table (stored in a separate function block).

Code listing 4. Code for estimation of the damping coefficient

```
#LN_Damping_Coef := ABS(LN((#An / #"An+1")));
#Damping_Coef := (#LN_Damping_Coefficient / (#Period_Time / 1000));
```

Seeking value of inclination is determined based on the equation of damped harmonic oscillations [3,4]:

$$x = A * e^{-\beta * t} * \cos(\omega_1 * t + \varphi) \tag{1}$$

where:

- A - amplitude of vibrations $[cm]$,
- β - damping coefficient,
- t - time $[s]$,
- ω_1 - frequency of damped vibrations $[\frac{rad}{s}]$,
- φ - initial phase value $[rad]$.

Correct operation requires an adequate coupling of hardware, software with control logic. For this purpose in the TIA PORTAL environment the WinCC for programming operator panels was used [2]. Described control modes have been presented in a graphical manner that creates simple visualization of the laboratory stand.

Figure 4 presents the view of an exemplary visualization of the operation mode used to optimization of pendulum vibrations. Status beam of the frequency inverter informs about the current state of the device, information are gathered from the PLC controller.

In order to enable a rapid response to changing the status of the device, beam area changes colour in accordance with a current state: operation (green), lack of permit to movement (orange), emergency stop (yellow).

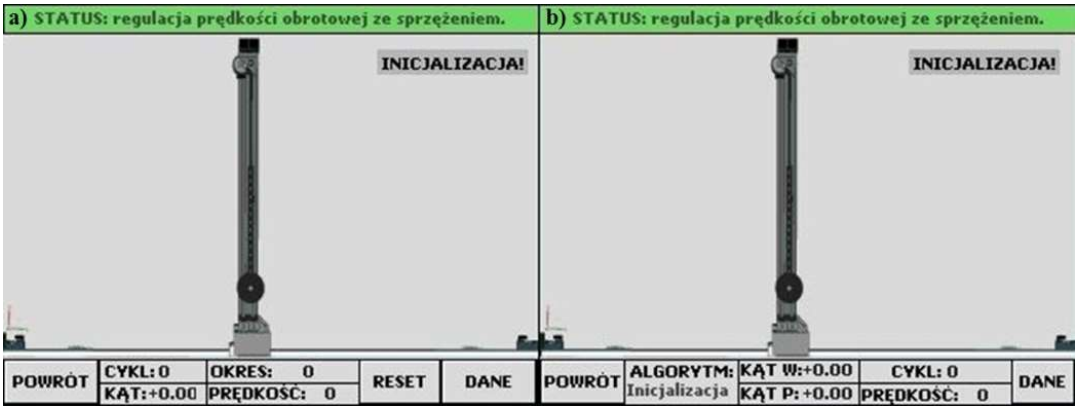

Fig. 4. View of vibration damping screen visualization: a) encoder mode, b) the algorithm of vibration damping

It is possible to activate the damping mode based on the current value indicated by the angle transducer (by choosing the Encoder button) and vibration damping (based on the predicted inclination angle).

3. Conclusions

Optimization of vibrations was realized for the rapid damping and preventing the formation of excessive vibrations of the pendulum.

Operation of swings optimization algorithm of the physical pendulum is based on feedback information from the rotation angle sensor (which is mounted in the axis of rotation). The laboratory stand can be controlled also via switches placed in the front plate of control box. The developed algorithms ensure adequate process control while achieving motion of pendulum without oscillations.

Communication between devices is made using industrial PROFINET network, which provides the required data rate. Through the implemented solutions founded tasks have been completed.

References

1. Bryan E.A, Bryan. L.A.: Programmable Controllers: theory and implementation. USA: Industrial Text Company, 1997.
2. Boyer S.: SCADA: Supervisory Control and Data Acquisition. USA: ISA, 2004.
3. De Silva C. W.: Mechatronics: an integrated approach. New York: CRC Press, 2005.
4. Mianowski B.: Determination of the period of small and large swings of physical pendulum. Lodz: Publishing House of Technical University of Lodz, 2009.
5. SEW-EURODRIVE: Programming Manual. Positioning and sequence control IPOSplus®. 1999.

SELECTED ENGINEERING PROBLEMS
NUMBER 7
INSTITUTE OF ENGINEERING PROCESSES AUTOMATION
AND INTEGRATED MANUFACTURING SYSTEMS

Mateusz SUMERA, Mariusz Piotr HETMAŃCZYK[1]

[1]Institute of Engineering Processes Automation and Integrated Manufacturing Systems, Faculty of Mechanical Engineering, The Silesian University of Technology, Gliwice, Poland
*mariusz.hetmanczyk@polsl.pl

SIMPLE ANGLE TRANSDUCER WITH ENHANCED RESOLUTION

Abstract: The article presents concept of simple angle transducer implemented for measurement of physical pendulum angular position. An introduction to the most commonly used transducers of angle of rotation was also described. The structure and the basic functional characteristics of developed transmitter were discussed. Another significant element is mounting in the laboratory stand used for optimization of swing values of the physical pendulum.

1. Introduction

Implementation of tasks associated with industrial drives positioning requires the use of complicated angle sensors. These sensors shall be characterized by a sufficiently large resolution (in order to obtain accurate information about the angular position of the machine), interference immunity (required for the measurement in harsh environment e.g. pollution, which in the case of sensors with optical systems may adversely affect the measured value). Angle transducers are used to [1,2]: a measurement of a speed (linear or rotational), obtaining information about the current position of movable elements, execution of reference movement, ensure a proper operation of drives using vector control algorithms.
In terms of action mode transducers can be divided into the following groups:

- incremental encoders - systems consisting of a shield and scanning elements (which may be optocouplers),
- absolute encoders - transmitters with memory of current position, even after turning off the power supply and fast change of position,
- resolvers - the most commonly used transducers in case of synchronous servo motors.

In case of a incremental encoder a disc transducer has on the perimeter two rows of holes with a determined spacing. Number of drill holes of the channel indicates encoder resolution, or accuracy of the measurement position. The measuring system is responsible for counting the number of pulses in order to obtain information about the current position.

An absolute encoder generates a coded signal corresponding to the position. An example is the absolute encoder with Gray coding, in which two successive code words differ only in the state of one bit. These transmitters can be divided into single-turn (which distinguish the

position of only one turn) and multi-turn (producing an output signal with information about the angular position and the number of revolutions).

Resolvers are constructed with stator and rotor windings. Rotor winding generates an alternating magnetic field that causes induction of the voltage in the two coils of stator (which are offset by 90). The voltage of one of the coils allows to determine the value of the cosine, while the second coil allows to determine the value of the sine of the angle of rotation. The ratio of voltages which are induced in individual windings depends on the rotor angular position [1,3].

2. Design of the angle transducer with enhanced resolution

In order to simulate a process of damping (in terms of different control algorithms realized by electric motors operated via frequency inverters) the model used to study a swing position of the physical pendulum was constructed. Described laboratory enables testing of advanced algorithms for damping of oscillations [6].

To meet requirements connected with obtaining information about the current position of the oscillator and implementation of damping algorithms the value of current angle of rotation is required. Outputs of described transducer are connected to a PLC controller. Due to the high cost of finished products the authors improve their own concept of incremental encoder. The two-channel transducer delivers pulses at different phase (Fig. 1), in order to determine the direction and angle of rotation of the physical pendulum.

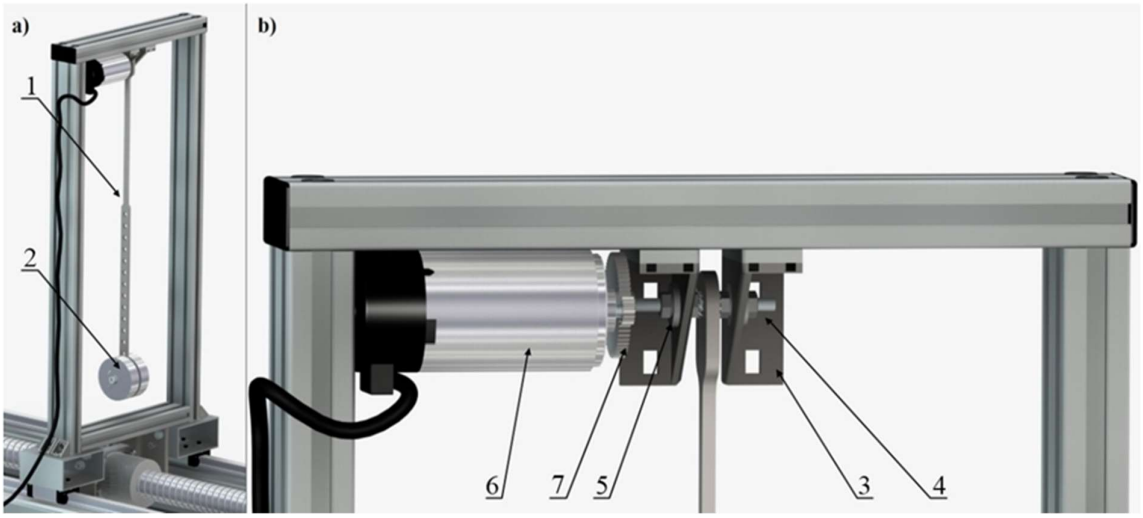

Fig. 1. View of the physical pendulum model: a) the frame, b) the clamping unit, where: 1 - the frame of the pendulum, 2 - test masses, 3 - mounting brackets, 4 - rotary axis, 5 - ball bearings, 6 - an encoder, 7 - a gear

Element used for generating pulses is a mechanical rotary winding pulser (Fig. 2). The system has three channels labelled A, B, C. Channel C is an input signal, which is based on the angle of rotation calculated on the basis of set at the inputs A and B. One turn generates 24 rising edges on the each of defined channel [7].

Constructed transmitter as an electronic system allows to work at a supply voltage of 5 Volts. On the other hand inputs signals of the most PLC controllers determine the value of the voltage according to the following ranges:

- 0÷5 [V] - logical zero,
- 6÷14 [V] - transient state,
- 15÷24 [V] - logical one.

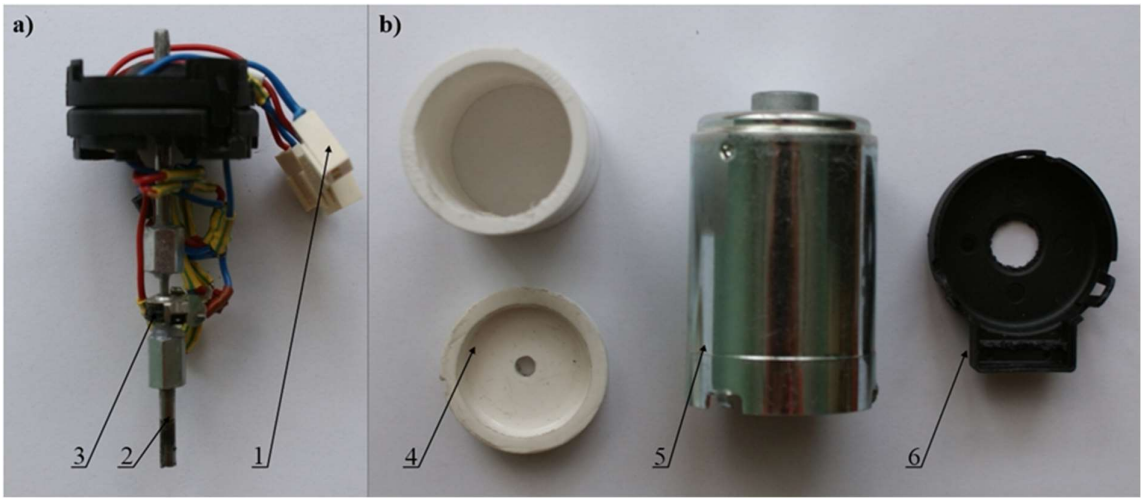

Fig. 2. View of encoder components: a) electronics, b) elements of the case, where: 1 - connection sockets, 2 - axis of the sensor, 3 - pulser, 4 - inner housing insulation, 5 - body, 6 - shielded wires

To ensure correct operation [5] of described encoder the authors used additional power source (changing of voltage to 24 Volts at the time of achieving a rising edge on any channel of encoder and sending the value to an input of a PLC controller). For this purpose, the technology of MOSFET N-type transistor (model BS170) was used, the operation of which is shown in Figure 3.

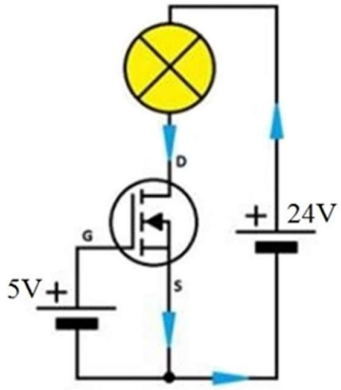

Fig. 3. Principle diagram of the MOSFET N transistor [4]

The transistors have three channels drain D, the goal G and the source S. The circuit compares the voltage found on a channel G and S at the moment the voltage from the encoder equals to 5 Volts. At the gate transistor facilitate a flow of voltage between the drain and the source, therefore it is possible to send required voltage to the PLC controller.

Control is made through voltage, therefore, the transmitter is equipped with the resistors to reduce the value of current intensities of described circuits (5 Volts - resistor 2.5 kΩ and 24 Volts- resistor 25 kΩ).

Due to the use of two-channel encoder, described relationship was performed twice. Created system has been assembled in a housing made of an insulating PVC (Fig. 2). As the body of a motor housing of DC was used. The housing is equipped with bushings in place of the support of the encoder axis.

Due to the low number of pulses generated between the axis of the physical pendulum and the encoder axis the author used a gear ratio of i=4 (Fig. 2). This results in 192 pulses per full revolution of the oscillator, i.e. generate a pulse occurs every 1,875˚.

3. Summary

The article shows an implementation of the incremental encoder designed to determine the angle of rotation of physical pendulum. Control of the angular position belongs to difficult tasks due to the necessity of obtaining a high-resolution, self-acquired data and the reliability of measuring equipment.

Presented concept has been made due to lack of angle transducers characterized by required parameters and dimensions. The basic features of the described solutions are simplicity of implementation, a low cost and an acceptable accuracy. On the other hand, it is also essential resistance to external conditions (determined by the housing).

The described solution has been implemented and tested. In conjunction with the control system and advanced algorithms the authors obtained an opportunity to test the influence of inclination angles at positioning accuracy of transported masses on gantries, cranes and other handling equipment .

References

1. SEW-EURODRIVE: Encoder Systems from SEW-EURODRIVE. 2009.
2. Fraden J.: Handbook of modern sensors - physics, design, applications. Springer-Verlag, New York 2004.
3. Hughes A.: Electric Motors and Drives Fundamentals, Types and Applications (3rd edition). Elsevier Linacre House, Oxford, 2006.
4. Leonhard W.: Control of Electrical Drives, Springer-Verlag, Berlin Heidelberg, 2001.
5. Dhillon B. S.: Engineering Maintenance - A Modern Approach. New York: CRC Press, 2002.
6. Gawronski W.K.: Advanced Structural Dynamic and Active Control of Structures. New York: Springer, 1998.
7. Kiameh P.: Electrical Equipment Handbook: Troubleshooting and Maintenance. New York: McGraw-Hill, 2003.

SELECTED ENGINEERING PROBLEMS
NUMBER 7
INSTITUTE OF ENGINEERING PROCESSES AUTOMATION
AND INTEGRATED MANUFACTURING SYSTEMS

Andrzej WRÓBEL[1]

[1]Institute of Engineering Processes Automation and Integrated Manufacturing Systems, Faculty of Mechanical Engineering, The Silesian University of Technology, Gliwice, Poland
*andrzej.wrobel@polsl.pl

FINITE ELEMENTS METHOD IN ANALYSIS OF SUBASSEMBLES AND ASSEMBLES OF THE FREIGHT CAR

Abstract: The main purpose of this article is to present an analysis of the laboratory stand designed to study the wall of wagons as well as analysis of the wall of the wagon itself. The stand was firstly used for testing models made of standard materials, and subsequently will be used for modifications of existing models involving, for example, the composite materials introduction in the analysed construction.

1. Introduction

Railway transport is one of the main factors of economic development in each country. Currently, two transport types are of particular importance: rail and road transport. The first one, due to the long time loading and unloading, is the most cost-effective on large distances in a transport of bulk cargoes. It loses its importance in the carriage of cargo, mainly locally and regionally on short distances because of the competitive road transport. This is mainly due to the relation of costs.

Energy consumption for dislocation of load unit in the road transport is 3-5 times bigger than in rail transport. The road transport allows direct carriage of goods from the sender to the recipient without the need for transhipment what introduce savings in time and cost. For the obvious advantages of rail transport belong mainly the short duration of transport, there is no traffic jams here and it is greener than road transport.

2. Object under examination

Designed laboratory stand will allow to the analysis of the Eaos 408W wagons shown in Figure 1. This is a top wagon with open container and universal application. It is primarily used to carry bulk cargo such as: coal, stone or wood. The loading is done manually or mechanically, by using a stationary load, while the unloading manually by the four pairs of doors, or mechanically on the so-called tippler [2, 3, 4].

Fig.1. Eaos 408W wagon [6]

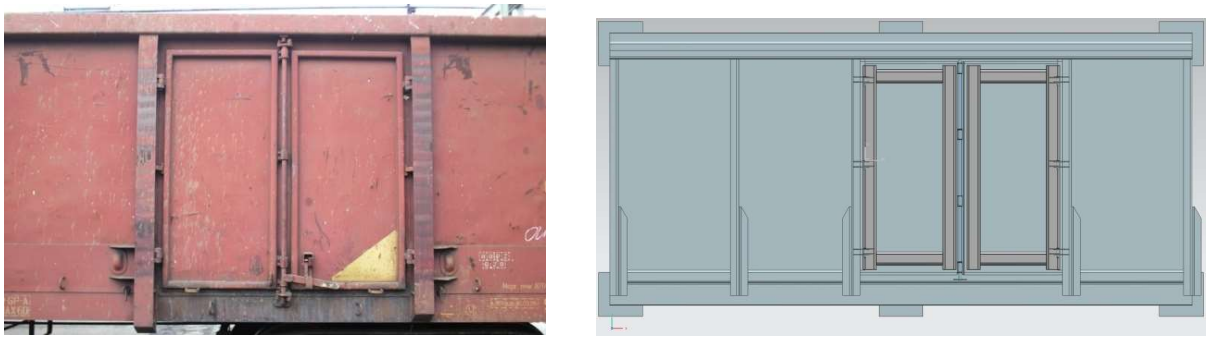

Fig.2. Analyzed part of the Eaos 408W wagon wall, a) real view, b) computer model

In general wagons walls are made of St3S steel. This is due to availability, price, strength of such material. The laboratory stand, together with the wall of the wagon model was designed according to the following design principles:

- The position was made in 1:4 scale,
- The position was made of steel sign St3S,
- Position allows you to ask hydraulic cylinder preset load,
- The simplified construction elements, that are crucial for analysis.

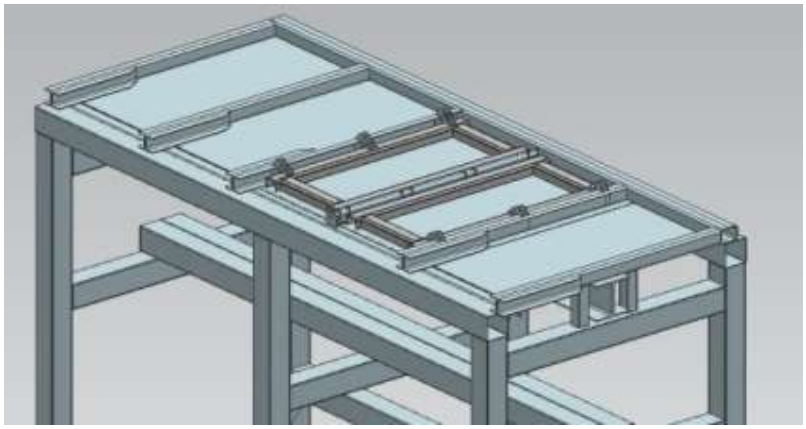

Fig.3. Computer model of the stand

To identify the state of stress in the wagon door it was assumed, that in order to carried out correct analysis, on the laboratory stand both, the door wagon and a part of construction elements should be mounted. It was shown in Figure 2.

3. FEM method in analysis of the computer model

In order to obtained value of displacement and stress of the object FEM strength analysis was conducted in Unigraphics software. Finite elements method (FEM) is the most common method for resolving the phenomena of complex mathematical character. The most important stage, in the analysis of this method, is so called discretization, so the imposition on the tested object elements with simple geometric shape depending on the analyzed surface. Finding of solution is closely linked with the computational power of computers and the numbers of finite elements, so from the complexity of the model. In many engineering cases, the discretization of the investigated technical object on elements is a simple matter, especially when we are dealing with simple constructions such as plates or grids. In complex cases, this division requires the designers knowledge and experience.

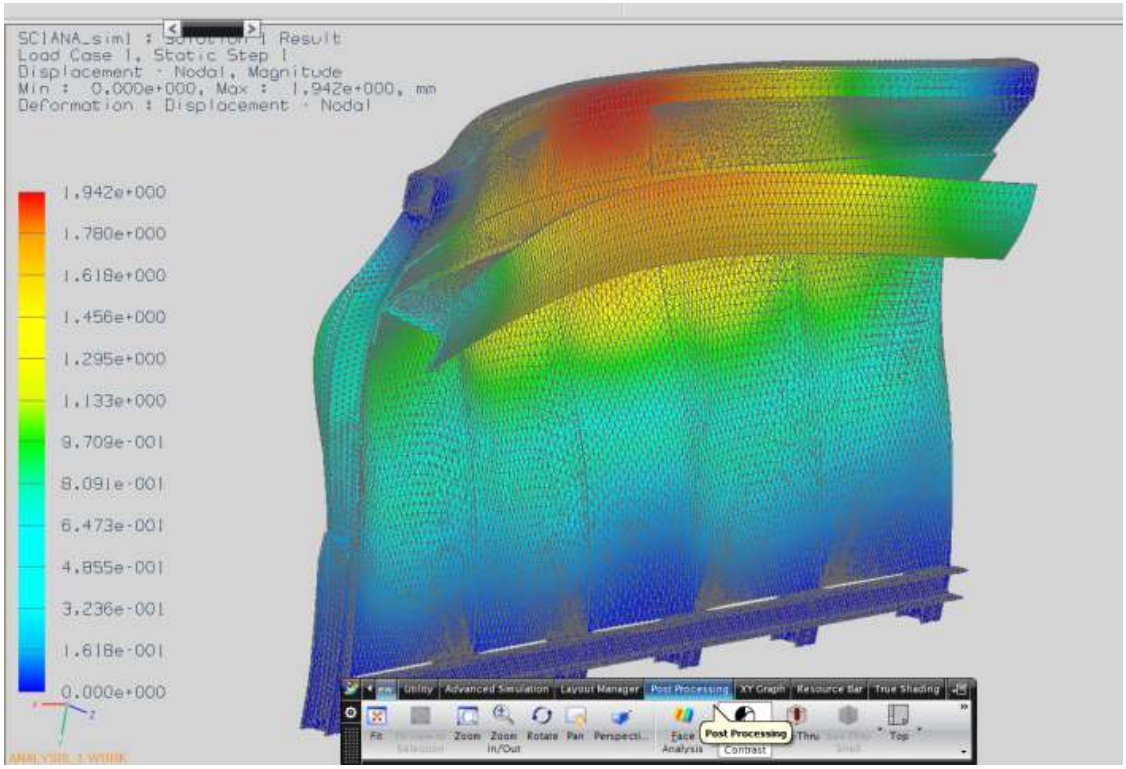

Fig.4a. FEM analysis of laboratory stand view 1

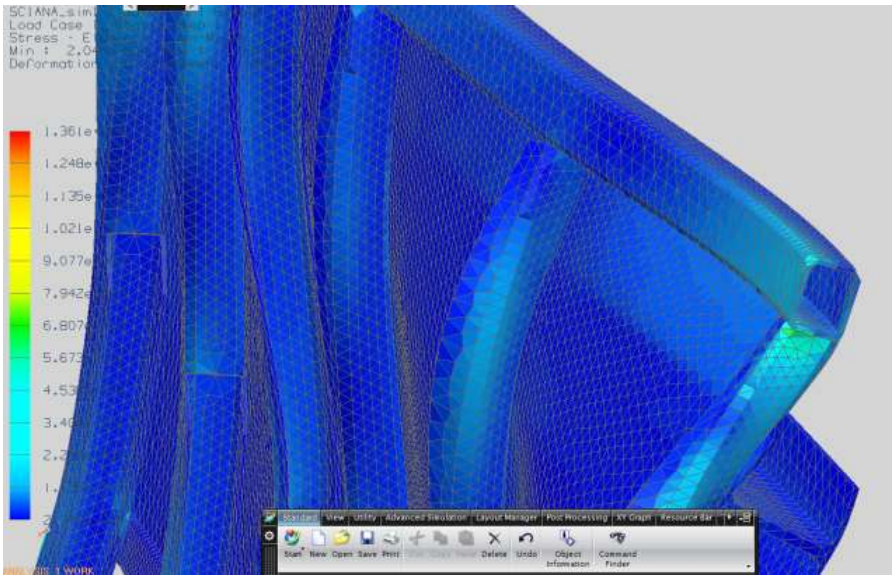

Fig.4b. FEM analysis of laboratory stand, view 2

In figure 4a and 4b were shown the object under examination. For the in which the applied exciting force equal to 25kN caused the maximum displacement, whose value does not exceed 1.8 mm. Comparing the stress values obtained after an analysis it was found that the limit values of steal are not exceeded by assuming loading.

This confirms the correctness of the geometrical parameters selection of metal profiles used to build a stand. In figure 5 was shown the wagon's wall, the largest displacements are marked in red color and are equal 1.9 mm.

4. Summary

In the presented paper, the modelling and analysis of the wagon's wall with the door and FEM analysis of laboratory used for those researches were described.

The stand and the test object was designed with the standard steel profiles in the 1:4 scale. The analysis was performed by finite elements method in Unigraphics program. It was found that size and shape of the profiles of both, the position and the whole wall of the wagon is valid under the assumption that the force value is 25kN and it is directed from the centre of the wagon.

The stand was designed for analysis of standard components. As a part of the future researches it is proposed application of composites or a composite-sheet metal combination in the wagons door.

References

1. Tarnowski W.: Construction engineering minor. Publisher Warsaw University of Technology, Warsaw 1977.
2. Jakubowski L.: Technology Work Load. Warsaw University of Technology Publishing House, 2003.
3. Chwesiuk K., Zalewski P.: Rail technology. Publisher Communications and Connectivity, Warsaw 1987.
4. Gąsowski W., Nowak R.: Studies of railway wagons. Publisher Poznan University ofTechnology 1989.

INDEX OF AUTHORS

Articles published on the basis of materials supplied by the authors.

ISSN 2299-954X

Journal published by Institute of Engineering Processes Automation and Integrated Manufacturing Systems, Faculty of Mechanical Engineering, Silesian University of Technology with number ISSN 2299-954X

Printed 150 copies Paper 80g Submitted for printing December, 2016